Assessing the Impact of Earth Observation Data-Driven Calibration of the Melting Coefficient on the LISFLOOD Snow Module

Valentina Premier[1,*], Francesca Moschini[2,4,*], Jesús Casado-Rodríguez[2], Davide Bavera[3], Carlo Marin[1], and Alberto Pistocchi[2]

[1]Institute for Earth Observation, Eurac Research, Bolzano, Italy.
[2]European Commission, Joint Research Centre (JRC), Ispra, Italy.
[3]Arcadia SIT, Milano, Italy.
[4]Rey Juan Carlos University, Madrid, Spain.
[*]These authors contributed equally to this work.

Correspondence: Valentina Premier (valentina.premier@eurac.edu) and Francesca Moschini (francesca.moschini@ec.europa.eu)

Abstract. LISFLOOD is a ~~comprehensive~~ large-scale operational hydrological model widely used in Europe. Among various hydrological processes, it simulates snowmelt using a ~~degree-day-based snow module. Traditionally,~~ degree-day approach, where the snowmelt coefficient is ~~calibrated using~~ typically calibrated against discharge data. This study evaluates LISFLOOD~~'~~'s current snow module and ~~explores~~ investigates an alternative calibration ~~approach~~ method based on Earth Observation (EO) ~~derived~~ snow cover fraction (SCF) ~~observations~~ across nine European basins with varying ~~degrees of snow cover~~ snow influence. We ~~utilize a novel integration of~~ integrate Sentinel-2 and MODIS data to address issues related to ~~data gaps and missed snow cover detection in complex topography~~gaps and misclassifications in snow detection over complex terrain. Using EO SCF, we estimate a spatially distributed snowmelt coefficient, ~~which contrasts with the uniform coefficients~~ in contrast to the uniform values currently used in LISFLOOD. The ~~new calibration approach, involving an optimization routine to match~~ coefficients are optimized by matching modeled and observed SCF, ~~outperforms a previous method that did not deal with fractional snow as well as discontinuous snow cover periods. When compared~~ and their hydrological impacts are assessed while keeping all other model parameters unchanged. This enables us to test whether modifying only the snowmelt coefficient affects discharge performance, and whether the standard calibration adequately represents both snow dynamics and streamflow. Compared with EO SCF, the ~~traditional calibration shows bias values ranging from -0.56% to 22.50% , with root mean squared error (RMSE) values varying from 20.43% to 54.64%. We obtained improvements up to 8% both in~~ standard calibration showed biases from –0.63% to 22.43% and RMSE values from 20.46% to 54.58%. The EO-based proposed approach improved both bias and RMSE ~~when the optimization approach is used. While~~ by up to 8%. Although the optimized coefficients did not significantly ~~alter simulated discharge~~ change the simulated discharge at the basin level, our analysis highlighted an effect in smaller upstream catchments. Moreover, the improved ~~SCA representation~~ representation of snow cover led in some cases to shifts in the timing and magnitude of snowmelt and total runoff. These findings highlight the potential of integrating EO data to ~~enhance snowmelt simulations and improve water balance predictions, with important implications for hydrological modeling and water resource management~~calibrate the snowmelt coefficient without changing other calibration parameters.

This approach may offer practical advantages in situations that require accurate snow cover representation, although our results show that standard calibration procedures provided an acceptable representation of snow dynamics.

1 Introduction

Snow cover plays a ~~crucial~~ critical role in hydrological processes, particularly in snow-fed regions ~~, where snowmelt significantly contributes~~ where snowmelt is a dominant contributor to river runoff. In mountainous ~~regions~~ and snow-dominated basins, snowmelt ~~often represents a major source of river discharge. Depending on geography and climate, the contribution of snow to river runoff can vary substantially, from as low as~~ can account for 40~~% up to~~ –95% of ~~the total annual flow~~ annual discharge, depending on geography and climate (Viviroli et al., 2007). This makes accurate ~~modeling of snowmelt processes essential for both flood forecastingand drought monitoringand prediction, especially in snow-dominated areas and in the context of a changing climate~~ snowmelt modeling essential for flood forecasting, drought monitoring, and long-term water resource management, especially under changing climatic conditions (Barnett et al., 2005; Blöschl et al., 2017; Beniston et al., 2011). ~~Hence, the snow module in hydrological models must be carefully designed and assessed for a correct management of water resources.~~

~~LISFLOOD is one of the most comprehensive operational models used in Europe to simulate hydrological processes (De Roo et al., 2000; Van Der Knijff et al., 2010; Burek et al., 2013). Developed by the European Commission's Joint Research Centre (JRC) for the Copernicus Emergency Management Service (CEMS), it is an integrated, distributed hydrological model that underpins both the European Flood Awareness System (EFAS) (JRC, 2024a; Matthews et al., 2025b) and the Global Flood Awareness System (GloFAS) (JRC, 2024b; Matthews et al., 2025a). LISFLOOD also supports the European and Global Drought Observatories (EDO and GDO) by providing key indicators (see) (Cammalleri et al., 2015, 2017). Primarily used for operational flood forecasting across Europe, LISFLOOD simulates several hydrological processes, including surface runoff, infiltration, groundwater recharge, and snowmelt. The snow module within LISFLOOD simulates the snowmelt through a temperature-based approach, specifically a degree-day model (Martinec and Rango, 1981). These relatively simple but robust models are commonly employed~~ Most hydrological models calibrate snow processes against streamflow observations. While effective for discharge simulation, this approach suffers from equifinality: multiple parameter sets can reproduce streamflow equally well but yield unrealistic representations of snow accumulation and melt (Beven, 2006, 2019). The problem is particularly pronounced in large-scale ~~hydrological models. The accuracy of the snow module is crucial for regions where snowmelt significantly impacts river flow. In most hydrological models, including LISFLOOD, the snow module is typically calibrated using discharge observation data. However, discharge data alone may not provide sufficient information to accurately identify all parameter values, particularly when dealing with distributed processes (Beven, 2012). On the other hand, calibration against spatially distributed, satellite-based snow cover data offers significant advantages in overcoming this limitation (Franz and Karsten, 2013)~~

. Snow cover area (SCA) from satellites has proven to be very accurate (e.g., Tedesco, 2015; Bormann et al., 2018). Nevertheless, models, where uniform calibration across diverse catchments compounds structural uncertainties (Beven, 2012). As a result, calibration based solely on discharge is insufficient for reliable snow-related applications.

Earth observation (EO) data provide an opportunity to address this limitation. Over the past 15 years, multi-objective calibration using both streamflow and satellite-derived snow cover has become state-of-the-art (Tang and Lettenmaier, 2010; Franz and Kar . However, whether such multi-objective calibration should remain the default, or whether alternative strategies can achieve a more realistic snow representation, remains an open methodological question.

In this study, we address this question using LISFLOOD, the coarse spatial resolution and the frequent cloud obstruction may limit detailed assessments, especially in complex and forested terrains (Riggs et al., 2015; Engel et al., 2017). By directly estimating the snowmelt coefficient from snow cover information, the calibration of other model parameters is simplified (Asaoka and Kominami, 2013; Riboust et al., 2019; Gyawali and Bárdossy, 2022; Ruelland, 2024). In the past, low-resolution products such as MODIS, which provides SCA at 500 m resolution, have been used for extensive comparisons of the LISFLOODsnow module (Thirel et al., 2012; Pistocchi et al., 2017). While the results have shown reasonable accuracy in validating snow models when considering SCA aggregated at the basin level, detailed analyses at the pixel level are lacking, especially when pixels present fractional snow cover during the melting period. Therefore, pixel-wise performances in terms of distributed hydrological model underpinning Europe's operational flood and drought monitoring systems (De Roo et al., 2000; Van Der Knijff et al., 2010; Burek et . Specifically, we focus on its temperature-index snow module and the snowmelt coefficient (C_m), following earlier efforts done by (Asaoka and Kominami, 2013; Riboust et al., 2019; Gyawali and Bárdossy, 2022; Ruelland, 2024). We test whether C_m can be directly estimated from EO snow cover fraction (SCF) should be assessed.

The aim of this work is to explore the capabilities and limitations of the snow module within the LISFLOOD modelin reproducing realistic snow cover distribution and accurate discharges across Europe. To accomplish this, we first assess the performance of the LISFLOOD snow module using a novel remote sensing snow cover product with a daily temporal resolution and 50 m spatial resolution. The SCA dataset is derived by fusing Sentinel-2 and MODIS data through gap-filling and downscaling techniques, which have shown high accuracy (Premier et al., 2021). Starting from a data after standard streamflow calibration, without re-calibrating the entire model. Using a novel high-resolution (HR) product preserves spatial detail even after aggregation, which is crucial for accurate modeling and analysis. A detailed evaluation of this dataset against other existing snow cover products highlighted its key strengths, particularly the availability of a fully gap-filled dailydataset. This novel dataset serves as a benchmark for evaluating the snow module's performances across Europe. 50 m, daily) EO binary snow product (Premier et al., 2021) to derive SCF, we evaluate: i) how well the current LISFLOOD setup reproduces snow and streamflow; ii) whether EO-derived C_m improves snow process realism; and iii) the impact of such adjustments on hydrological performance across diverse European catchments.

Secondly, this paper focuses on the snowmelt coefficient calibration — a key parameter within the simplified snowmelt model of LISFLOOD . We propose a dedicated calibration of the coefficient by using spatially distributed snow cover information derived from earth observation (EO) data as a benchmark. This calibration approach differs from traditional hydrological calibration methods by introducing an independent process that does not rely solely on discharge data. Furthermore, the The snowmelt coefficient is estimated on a pixel-by-pixel basis ~~, enhancing the accuracy of snowmelt representation across different landscapes. This represents an important improvement over the LISFLOOD approach , which results in a lumped coefficient, constant for each subcatchment. This study proposes to calibrate the snowmelt coefficient using: i) a previously proposed method based on the number of snow-covered days per pixel for estimating the coefficient (Pistocchi et al., 2017), and ii) a novel method~~ by applying an optimization approach that minimizes the error between LISFLOOD SCF and EO SCF. ~~The second~~ This is possible thanks to the introduction into the calibration process of i) an appropriate parameterization to convert ~~SWE to SCF~~snow water equivalent (SWE) to SCF (Swenson and Lawrence, 2012), and ii) the use of a daily gap-filled SCF time-series based on high-resolution (HR) EO binary snow cover data (Premier et al., 2021). The spatialized coefficient represents an important improvement over the standard LISFLOOD approach, which consists in a lumped coefficient, constant for each subcatchment. Also, the use of HR EO snow cover data represents a step forward w.r.t. previous studies that made use of low-resolution products such as MODIS (500 m) (Thirel et al., 2012; Pistocchi et al., 2017). Finally, we re-run the model using the EO-derived snowmelt coefficient, with all other settings consistent with the standard setup to specifically assess the effects of a more consistent representation of the snow module on hydrological response.

The study sites encompass a variety of watersheds selected to represent diverse topographical and climatic conditions across Europe, including major mountain ranges and a wide range of latitudes. These basins also feature different land cover types, from rugged mountainous terrain to flat, forested areas, offering a comprehensive foundation for evaluating the model's performance in diverse environmental contexts. Although demonstrated here for LISFLOOD, the approach is general and transferable to other large-scale hydrological models.

2 ~~Material and~~ Methods

Our methodology combines EO snow cover data with the LISFLOOD hydrological model to evaluate and improve the representation of snow processes. The workflow is illustrated in Fig. 1.

Daily high-resolution (50 m) binary snow cover data are used to derive SCF time series (hereafter EO-SCF; Sec. 2.1) . In parallel, the LISFLOOD snow module (Sec. 2.2) is run to simulate SWE. A parameterization is then applied to transform SWE into modelled SCF (hereafter L-SCF; Sec. 2.3), enabling direct comparison with EO-SCF. The snowmelt coefficient (C_m) is treated as a free parameter of the snow module. We estimate C_m by minimizing the difference between L-SCF and EO-SCF through an optimization procedure (Sec. 2.4). For each year, we obtain a spatially-distributed coefficient (EO-C_m). A pixel-wise average over time is then computed. One season is excluded from calibration and used only for evaluation. In the final LISFLOOD re-run, the discharge-calibrated coefficient (L-C_m) is replaced by EO-C_m. For clarity, all acronyms used throughout the manuscript are summarized in Table 1.

2.1 Daily Snow Cover Area Retrieval

~~Given the~~ EO optical observations have proven highly accurate for snow monitoring (e.g., Tedesco, 2015; Bormann et al., 2018) , yet their applicability is limited by sensor constraints and environmental factors (Riggs et al., 2015; Engel et al., 2017). A

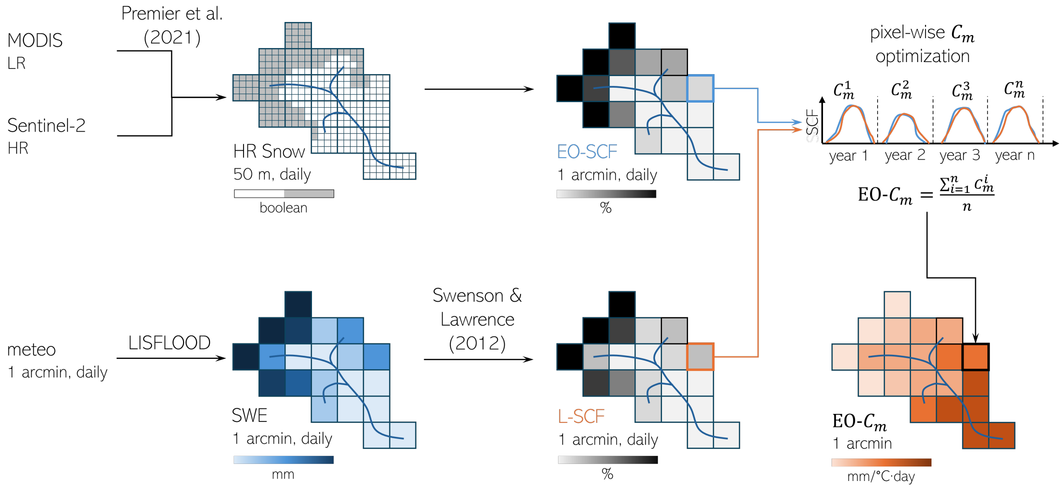

Figure 1. Workflow of the methodology.

Table 1. List of acronyms used in this study.

Acronym	**Meaning**
EO-SCF	Snow cover fraction (SCF) derived from Earth Observation (EO) data and used here as reference.
L-SCF	Snow cover fraction (SCF) derived from the LISFLOOD snow module. SWE is first simulated and then converted to SCF using a snow-cover parameterization.
EO-C_m	Snowmelt coefficient (C_m) obtained from calibration against EO data - spatially distributed.
L-C_m	Snowmelt coefficient (C_m) obtained from the standard calibration against discharge data - lumped.

primary challenge is the trade-off ~~between spatial and temporal resolution in current multi-resolution satellite missions, there is a shortage of daily high-resolution (HR) optical data necessary for effective snow cover change monitoring~~ between spatial and temporal resolution. Low-resolution (LR) sensors, such as MODIS ~~and~~ or VIIRS, provide daily ~~SCF data, but their coarse spatial resolution limits their effectiveness~~ estimates of snow cover fraction (SCF) but lack the spatial detail required in complex alpine ~~and heterogeneous environments, where finer detail is essential~~ terrain (Molotch and Margulis, 2008). In contrast, ~~HR multispectral sensors, like~~ high-resolution (HR) sensors, such as Sentinel-2, ~~offer more spatially detailed snow cover data,~~

but their lower revisit frequency, due to orbital constraints, reduces their utility for continuous monitoring of capture fine-scale spatial patterns but have infrequent revisit times, making them less suitable for tracking rapidly changing snow conditions.

dynamics. Additionally, all optical sensors face challenges due to are affected by persistent cloud cover, which can obscure the ground for extended periods and hinder snow detection. This is particularly problematic creates substantial data gaps—particularly in mountainous regions , where snow patterns are highly variable (Parajka and Blöschl, 2006). Currently available operational products struggle to overcome these limitations, leading to significant data gaps. To address this issue, we integrate multi-resolution optical satellite data to obtain daily HR SCA information, specifically binary data indicating snow presence. We apply the approach presented by Premier et al. (2021)to fill temporal and spatial gaps. The approach to creating (Parajka and Blöschl, 2006) . Consequently, standard operational products are often incomplete and inconsistent, limiting their utility for hydrological applications.

To address these limitations, we adopt the approach of Premier et al. (2021), which integrates LR and HR optical satellite observations to produce a continuous, gap-filled daily SCA dataset relies on two primary data sources, i.e. , i) a LR SCF product based on optical data, as MODISdata, gap-free daily binary snow dataset (snow/snow-free) at HR (50 m). The method combines i) LR daily SCF products (e.g., MODIS) and ii) HR optical data, particularly Sentinel-2 snow maps . The methodology builds on the intuitive idea within an iterative gap-filling and downscaling framework, followed by a machine learning correction step. This framework relies on the assumption that inter-annual spatial patterns are snow patterns are strongly influenced by local topography and meteorological conditions. Areas with similar (elevation, slope, and aspecttend to exhibit comparable responses to snow processes, such as accumulation , distribution, and melting. A long time series aspect) and meteorological conditions, resulting in recurrent spatial patterns of snow accumulation and ablation. By leveraging a long archive of HR acquisitionsis required to learn the recurring patterns. The workflow leverages this concept through an iterative gap-filling and downscaling procedure, followed by a machine learning step. Importantly, the approach is designed to be independent of the HR or LR input snow cover product. In this study, our focus will be on operationally available datasets with the main aim to broaden the potential use of this approach. For more details on the daily SCA retrieval approach, refer to Premier et al. (2021) , the method reconstructs daily HR snow maps while correcting for known LR limitations, including errors from grain size variability, solar zenith angle, viewing geometry, and atmospheric effects. Details about the performance of the algorithm can be found in the original work.

Once the HR daily gap-filled SCA binary snow cover is derived, it is HR binary snow maps are generated, they are aggregated and resampled to the grid of the LISFLOOD model resulting in an SCF value LISFLOOD model grid to derive daily SCF values for each pixel. We refer to this time-series as EO-SCA. Appendix A details the HR and LR snow cover data used to retrieve daily snow cover in this study, and provides further insights into the use of alternative time series as EO-SCF. Importantly, starting from HR products preserves finer details even after aggregation, which is crucial for accurate modeling and analysis. Using HR data allows for better detection of the fractional snow linked for example to small-scale snow patches often missed in LR datasets, providing substantial improvements during the melting period, which is the main focus of this study.

A detailed description of the input datasets and a comparison with alternative operational gap-filled ~~snow cover datasets that are operationally available~~products is provided in Appendix A. Evaluation against other existing snow cover products highlights the key strengths of this approach, notably the availability of a fully gap-filled daily HR dataset.

2.2 ~~Snow Module of~~ The LISFLOOD Model

LISFLOOD is an open-source, spatially distributed hydrological model designed to simulate ~~hydrological processes in large European river basins . The model simulates the whole water cycle and comprises multiple modules to reproduce various hydrological processes such as surface runoff, infiltration, groundwater recharge, and snowmelt. A complete description of the model is provided by De Roo et al. (2000); Van Der Knijff et al. (2010); Burek et al. (2013)~~the complete water cycle in large river basins (De Roo et al., 2000; Van Der Knijff et al., 2010; Burek et al., 2013). Developed by the European Commission's Joint Research Centre (JRC) for the Copernicus Emergency Management Service (CEMS), it underpins both the European Flood Awareness System (EFAS) (JRC, 2024a; Matthews et al., 2025b) and the Global Flood Awareness System (GloFAS) (JRC, 2024b; Matthews et al., 2025a), and supports the European and Global Drought Observatories (EDO and GDO) by providing key hydrological indicators (Cammalleri et al., 2015, 2017) (see https://drought.emergency.copernicus.eu/). The current ~~model setup operates~~ EFAS and EDO setup (v5.0) operate on a 1 arc-minute grid ~~resolution~~ (approximately 1.4 km), covering the ~~entire~~ European Union, the European continent, and the Mediterranean coast, while GloFAS and GDO operate globally at 3 arc-minute resolution. The model includes multiple process modules, including surface runoff, infiltration, groundwater recharge, and snow dynamics. It can be applied at multiple scales, from large river basins to global regions, supporting flood forecasting, water resource assessments, and ~~analysis of factors like~~ analyses of water demand, river regulation, land-use changes, and climate change. ~~Precipitation~~

2.2.1 EFAS5 Setup

In this study, we refer to the EFAS5 setup, which is forced by precipitation and temperature fields ~~used as input for the model are~~ from the EMO-1 dataset (Thiemig et al., 2022)~~, used as forcing in the EFAS. At the moment, the model is the core component of the European operational flood and drought monitoring and forecasting system within the CEMS. The same applies at a global scale (3 arc-minute resolution) for GloFAS, EDO and GDO.~~

~~The model is calibrated on~~. In the standard LISFLOOD calibration, 14 ~~parameters,~~ model parameters—including the snowmelt coefficient~~,~~—are optimized to reproduce observed river discharge by using the Distributed Evolutionary Algorithms in Python (DEAP) (Fortin et al., 2012)~~. The optimization is based on~~, with the modified Kling-Gupta Efficiency (KGE) (Kling et al., 2012) ~~objective function, calculated from simulated and observed river discharge.~~

$$KGE = 1 - \sqrt{(r-1)^2 + (\beta-1)^2 + (\gamma-1)^2}$$

~~where β is the bias ratio (Eq. ??), γ is the variability ratio (Eq. ??) and r is the Pearson correlation.~~

$\beta = \mu_s / \mu_o$

$$\gamma = \frac{\sigma_s/\mu_s}{\sigma_o/\mu_o}$$

μ_s and μ_o are simulation and observation mean, σ_s and σ_o are simulation and observation standard deviationas the objective function. Details on the calibrated parameters and their ranges are available at: https://ec-jrc.github.io/lisflood-code/4_annex_parameters/.

When multiple stations are available within a catchment, the calibration process employs follows a cascading approach. The basin is partitioned into inter-catchments: the basin is divided into subcatchments, and each inter-catchment is calibrated sequentially from upstream to downstream. The parameters Parameters for ungauged basins are estimated using a regionalization approach (Beck et al., 2016), whereas while coastal and endorheic catchments (area below $<$ 150 km^2) use default parameters. Note that the calibration assigns values. Each parameter is assigned a single value to each parameter across all pixels within an inter-catchmentsubcatchment. The snowmelt coefficient obtained through this standard procedure is referred to as L-C_m.

For the purpose of In this study, we will focus exclusively on recalibrate only the the snowmelt coefficient, integrated in the snow module and, in detail, on the snowmelt coefficient. In LISFLOOD, the SWE is calculated by accounting for both of the model, against EO data (see Sec. 2.4). The remaining 13 parameters are kept unchanged, following the EFAS5 setup. After obtaining the new snowmelt coefficient, the accumulation and melting processes: LISFLOOD model is re-run. We deliberately chose to avoid re-calibrating the model in this study. Our objective was to isolate and assess the direct impact of a snowmelt coefficient calibrated independently from the conventional calibration procedure on simulated river discharge. This approach allows us to determine whether modifying the snowmelt coefficient alone produces significant effects on discharge, and to test whether the existing snow calibration in LISFLOOD yields acceptable results for both snow dynamics and river flow simulations. A more detailed explanation of the methodology and criteria used to evaluate the LISFLOOD model outputs is provided in Sec. 4.4.

$\text{SWE} = P_{snow} - M$

2.2.2 LISFLOOD Snow Module

where P_{snow} is the solid precipitation and M is the snow melt, both of them expressed in mm. The total precipitation is split in solid precipitation P_{snow} and rain R Since the snowmelt coefficient is the focus of this study, we provide a detailed description of the snow module. LISFLOOD simulates snowmelt using a temperature-based approach — specifically, a degree-day model that also accounts for enhanced melt during rainfall events (Speers and Versteeg, 1982).

The SWE is computed by accounting for both accumulation and melt processes. Total precipitation is partitioned in rainfall (P_{rain}) or solid precipitation (P_{snow}) based on a temperature threshold that is set ~~as~~ to $1^\circ C$. ~~The melting is given by the following equation:~~

Two melt processes are modeled: snowmelt (SM) and icemelt (IM). All the variables listed above are expressed in mm.

$$~~M~~\mathrm{SWE}_t = \max\left(0, \mathrm{SWE}_{t-1} + P_{\mathrm{snow}} - \mathrm{SM} - \mathrm{IM}\right) \tag{1}$$

~~where $C_m[\frac{mm}{^\circ C\cdot day}]$ is~~ Snowmelt (SM) occurs when the average temperature ($T_{\mathrm{avg}}[^\circ C]$) exceeds a threshold ($T_m[^\circ C]$), which is set to $1^\circ C$. The rate of melt is controlled by the snowmelt coefficient~~or degree-day factor,~~ , which is partitioned into a fixed term ($C_m[\frac{mm}{^\circ C\cdot day}]$) and a seasonal term ($C_{seas}[\frac{mm}{^\circ C\cdot day}]$~~is a degree-day factor introduced to account for seasonal effects, $R[\frac{mm}{day}]$ is the rainfall intensity, $T_{avg}[^\circ C]$ is~~). The focus of this study is the calibration of that fixed term (C_m). The seasonal term (C_{seas}) allows for a sinusoidal variation of the snowmelt coefficient of $\pm 0.5\frac{mm}{^\circ C\cdot day}$ depending on the day of the year (doy). To account for increased snowmelt under rain, the ~~average daily temperature, $T_m[^\circ C]$ is the temperature threshold at which snowmelt occurs — set as~~ snowmelt coefficient is further increased by 1 ~~$^\circ C$ — and $\Delta t[days]$ is the time interval~~ % per mm of rainfall (P_{rain}).

$$\mathrm{SM} = \begin{cases} (C_m + C_{seas}) \cdot (1 + 0.01 \cdot P_{\mathrm{rain}}) \cdot (T_{\mathrm{avg}} - T_m) \cdot \Delta t, & \text{if } T_{\mathrm{avg}} > T_m \\ 0, & \text{if } T_{\mathrm{avg}} \leq T_m \end{cases} \tag{2}$$

$$C_{seas} = \frac{1}{2}\sin\left(\frac{2\pi}{365.25}(\mathrm{doy} - 81)\right) \tag{3}$$

Icemelt (IM) reproduces the snow depletion at high altitudes, where temperature rarely exceeds the melting threshold (T_m). It is constrained to the summer season —~~set as 1 day. The degree-day factor for the seasonal effects is computed as follows:~~

~~$$C_{seas} = \frac{1}{2}\sin\left(\frac{2\pi}{365}(\mathrm{doy} - 81)\right)$$~~

from June 13 (start) to September 13 (end) in the Northern Hemisphere. The process is controlled by the seasonally-varying icemelt coefficient (C_{im}), which has a maximum value of $7\frac{mm}{^\circ C\cdot day}$.

$$\mathrm{IM} = \max\left(0, C_{im} \cdot T_{\mathrm{avg}} \cdot \Delta t\right) \tag{4}$$

~~Note that the sum $C_m + C_{seas}$ must remain positive. Since C_{seas} fluctuates between -0.5 and 0.5, C_m must be at least 0.5 to ensure this condition is satisfied. Furthermore, snow melt and accumulation are modeled separately for 3 separate elevation zones to take into account sub-pixel heterogeneity linked to elevation differences given the large pixel size. The~~

$$C_{im} = \begin{cases} 7 \cdot \sin(\frac{4\pi}{365.25} \cdot (\mathrm{doy} - \mathrm{start})), & \text{if start} < \mathrm{doy} < \text{end} \\ 0, & \text{else} \end{cases} \tag{5}$$

Due to the often coarse spatial resolution in LISFLOOD, the elevation differences within a pixel can be significant, which in turn affects snow processes. To overcome this limitation, LISFLOOD subdivides each pixel into three elevation zones. It simulates snow accumulation and ablation in each of those zones and then aggregates the results to obtain the pixel-level SWE. A normal distribution is applied to the digital elevation model from the 90 m Multi-Error-Removed Improved-Terrain (MERIT) (Yamazaki et al., 2017) to divide the pixel in three elevations zones of equal area. The average temperature is corrected for the upper and lower elevation zones using a fixed lapse rate of $0.0065\frac{°C}{m}$.

For more details, the model code and documentation are available at https://ec-jrc/.github.io/lisflood/.

2.3 Snow Cover Parametrization

To compare the SWE output of the LISFLOOD model with the EO-SCA, it is necessary to convert SWE into SCFLISFLOOD's SWE output with EO-SCF, SWE must be converted into snow cover fraction (SCF). This conversion implies the use of requires a parametrization that accounts for changes variations in snow depth and density within a pixel. Due to the large substantial intra-pixel variability, the relation relationship is influenced by factors such as topography and land cover (Roesch et al., 2001). Several parametrizations are available parameterizations have been proposed in the literature (Lee et al., 2024) (e.g., Liston, 2004; Niu and Yang, 2007; Helbig et al., 2015; Pimentel et al., 2017; Lee et al., 2024). In this study, we adopted the approach adopt two approaches that balance model complexity with data availability. The first, proposed by Swenson and Lawrence (2012) used and implemented in the Community Land Model (CLM). However, the approach of Zaitchik and Rodell (2009) was also tested and the results can be found in Appendix, is relatively sophisticated. The second, introduced by Zaitchik and Rodell (2009), is a simpler empirical method requiring fewer inputs but has been shown to provide consistent results. For brevity, and given their similar performance, details and results from the second approach are provided in Appendix B.

Swenson and Lawrence (2012) differentiates the accumulation and ablation periods. The updated snow cover fraction SCF^{n+1} For the accumulation, the SCF after a precipitation event can be interpreted probabilistically. In a simple linear formulation, the probability of a pixel to be snow covered or the SCF is given by the following equation for accumulation formula:

$$\mathrm{SCF}^{n+1} = 1-(1-\tanh\min(1, k_{accum}\Delta\cdot\mathrm{SWE}))(1-\mathrm{SCF}^{n}), \tag{6}$$

where k_{accum} [1/mm] is a scaling parameter that relates SWE to SCF. Accordingly, the probability that a pixel remains snow-free is a constant with a default value of 0.1, $1-\mathrm{SCF}$. For multiple independent snowfall events, the cumulative probability that a pixel remains snow-free is the product of the individual probabilities. Therefore, after $N+1$ events, the cumulative SCF is

$$\mathrm{SCF}_{N+1} = 1-\prod_{i=0}^{N}(1-\mathrm{SCF}_i). \tag{7}$$

A more refined, probabilistic formulation for accumulation uses a hyperbolic tangent function, which ensures that SCF asymptotically approaches 1 as SWE increases, to update SCF after each event:

$$\mathrm{SCF}^{n+1} = 1 - \left[(1 - \tanh(k_{accum}\,\Delta\mathrm{SWE}))(1 - \mathrm{SCF}^{n})\right], \tag{8}$$

where ΔSWE is the amount of new SWE in mm~~and SCF^n is the snow cover fraction from the previous time step~~. Although many state-of-the-art models assume a constant value for k_{accum} ~~, our results indicate that this parameter significantly influences the outcome and~~ equal to 0.1, it likely varies pixel-wise due to topographic differences. The parameter k_{accum} can be estimated by measuring SCF and ΔSWE ~~when precipitation occurs~~ during precipitation events over an initially snow-free area, as suggested by Swenson and Lawrence (2012). To identify such ~~a condition~~conditions, we selected the first day on which both ~~EO-SCA and LISFLOOD simulation indicate snow presence. If a pixel never exhibits~~ EO-SCF observations and LISFLOOD SWE are greater than 0 (snow presence). Equation 8 is then inverted to obtain an estimated value of k_{accum}. The parameter is constrained to a maximum of 0.5, consistent with what reported in the original study. For pixels that never exhibit snow, the default value is retained. This ~~process~~ procedure was repeated for all ~~available~~ calibration seasons, and ~~an averaged value over time was then considered~~the final pixel-wise value of k_{accum} was taken as the average over time. The obtained parameters are reported in Appendix B in Fig. B1.

~~On the other hand,~~ For the melting period, Swenson and Lawrence (2012) relate SCF ~~is given by the following equation for melting~~ to the dimensionless snow water equivalent scaled by the maximum SWE ($\mathrm{SWE}_{\mathrm{max}}$) through the following empirical equation:

$$\mathrm{SCF} = 1 - \left[\frac{1}{\pi}\arccos\left(2\frac{\mathrm{SWE}}{\mathrm{SWE}_{\mathrm{max}}} - 1\right)\right]^{N_{melt}} \tag{9}$$

where ~~$\mathrm{SWE}_{\mathrm{max}}$ is the threshold SWE above which SCF is 100% - it depends on the topography and the forest coverage of the pixel - and~~ N_{melt} is a parameter that depends on the topographic variability within the grid cell~~and~~. It is calculated as follows:

$$N_{melt} = \frac{200}{\max\left(10, \sigma_{topo}\right)} \tag{10}$$

with σ_{topo} being standard deviation of the elevation within a grid cell calculated from the ~~Multi-Error-Removed Improved-Terrain (MERIT)~~ MERIT DEM with a spatial resolution of 90 m (Yamazaki et al., 2017). ~~The threshold~~ When an accumulation follows a melting event, $\mathrm{SWE}_{\mathrm{max}}$ ~~is updated when accumulation happens as follows~~

~~$$\mathrm{SWE}_{\mathrm{max}} = \mathrm{SWE}\left[\frac{\cos(\pi(1-\mathrm{SCF})^{1/N_{melt}}) + 1}{2}\right]$$~~

2.4 ~~Snowmelt Coefficient Estimation from EO Data~~

~~The snowmelt coefficient is estimated following two different approaches. First, the approach presented by Pistocchi et al. (2017) . Under the hypothesis of a period of continuous snow cover, we can write the following balance of snowfall and snowmelt:~~

needs to be updated to re-define a consistent depletion curve. This is done by inverting Eq. 9 and using the following equation:

$$\sum_{i=1}^{n}(P_{snow,i}-M_i)\text{SWE}_{\text{max}} = 0\text{SWE}\left[\frac{\cos(\pi(1-\text{SCF})^{1/N_{melt}})+1}{2}\right] \tag{11}$$

where n is the number of days composing the continuous snow cover period. By substituting with Eq. 2, we can derive the snowmelt coefficient

$$C_m = \frac{\sum_{i=1}^{n} P_{snow,i} - \sum_{i=1}^{n} C_{seas}(1+0.01\cdot R_i\cdot\Delta t)(T_{avg,i}-T_m)\cdot\Delta t}{\sum_{i=1}^{n}(1+0.01\cdot R_i\cdot\Delta t)(T_{avg,i}-T_m)\cdot\Delta t}$$

The periods of continuous snow cover are detected from EO-SCA. While Eq. C1 may not strictly apply to pixels experiencing multiple snow cover/snow-free cycles (common at lower altitudes or temperate climates), we simplify the analysis by assuming its validity for all snow-covered days. This simplification also helps mitigate residual errors from inaccurate SCA reconstructionFor more details, refer to the original code at https://github.com/ESCOMP/CTSM/blob/master/src/biogeophys/SnowCoverFractionSwensonLawrence2012Mod.F90, which implements the snow cover fraction parameterization by Swenson and Lawrence (2012) .

An alternative approach for estimating the melting coefficient involves formulating

2.4 Snowmelt Coefficient Estimation from EO Data

The snowmelt coefficient is estimated by solving an optimization problem aimed at minimizing that minimizes the error between LISFLOOD L-SCF and EO-SCF. This procedure aims to align model outputs with observations, thereby increasing the realism of the simulation results. We remark that L-SCF is derived from modeled SWE using Eq. 1 and the parametrization defined in Eqs. 8 and 9, with C_m treated as a free parameter in this optimization phase. Specifically, we minimize the mean squared error (MSE) over time to identify the optimal coefficient that results in the smallest error. Hence, we solved produces the smallest discrepancy. Accordingly, the following minimization problem is solved for each pixel to obtain the EO-based snowmelt coefficient:

$$\text{EO-}C_m = \arg\min_{C_m} \sum_{t\, t\in\mathcal{T}_{\text{hy}}} (\text{L-SCF}(t, C_m) - \text{EO-SCF}(t))^2 \tag{12}$$

where $\hat{C_m}$ is the optimized snowmelt coefficientand L-SCF is calculated from SWE through Eq. 1 and by applying the parametrization (Eqs. 8 and 9)The optimization is performed on a pixel-wise basis over all time steps within a given hydrological year $\mathcal{T}_{\text{hy}}$ to obtain a single, time-invariant coefficient. To solve this optimization problem, we utilize the L-BFGS-B algorithm -—a limited memory quasi-Newton, gradient-based optimization algorithm-— provided in the SciPy library (Virtanen et al., 2020).

The snowmelt coefficient is estimated in both cases on a pixel-wise basis for each hydrological season. Estimated values are constrained between 0.5 and 10, as values outside this range lack physical meaning and may result from errors, such as having too few days to perform a reliable optimization (e.g., ephemeral snow at low altitudes). Specifically, according to Eq. 2, lower values of C_m would result in negative melting, which is not physically realistic. ThenSubsequently, a mean value for each pixel is calculated using data from all seasons except the final one (2022-2023), which is used exclusively for a further independent assessment of the results. For pixels where the coefficient could not be estimated - —such as those without snow during the year or where pixels were masked out due to the presence of water bodies- the original LISFLOOD coefficient is retained— L-C_m is retained.

We also considered an alternative, simpler approach previously presented by (Pistocchi et al., 2017). Like the main method, it relies on EO data but is based solely on the number of snow-covered days. For brevity, details and results are provided in Appendix C.

2.5 Assessment of the Results

The obtained EO-C_m is first evaluated qualitatively against L-C_m. A correlation analysis is also performed against selected topographic, geographic, and land cover features. For a quantitative assessment, we compare the resulting snow-covered area (SCA), defined as the percentage of the basin covered by snow. To do this, SWE is simulated using the LISFLOOD snow module (Eq. 2) with both L-C_m and EO-C_m. The simulated SWE is then converted to SCF (see Sec. 2.3) and aggregated to the basin level to obtain SCA. The SCA obtained using L-C_m is denoted as L-SCA L-C_m, while that obtained using EO-C_m is denoted as L-SCA EO-C_m. These model-based estimates are then compared against EO-SCA, derived from EO-SCF, which serves as the benchmark. The results are reported in Sec.4.1.

We also evaluate improvements at the pixel scale by computing metrics for SCF, using EO-SCF as the benchmark. Specifically, we calculate bias, root mean squared error (RMSE), and correlation between L-SCF (using both L-C_m and EO-C_m) and EO-SCF. Metrics are first computed per pixel over time and then averaged spatially across the basin. To focus on the model's ability to detect snow, we exclude pixels where both modeled and observed SCF are zero (i.e., snow-free conditions). Including such pixels would artificially inflate performance metrics, particularly during periods when large portions of the basin are snow-free, thereby biasing the results. An analysis of the correlation with the errors versus physiographic and climatic features is also performed, together with an evaluation of the seasonal error trends. SCA results are reported in Sec.4.2.

A SWE intercomparison is performed for basins where a reference dataset is available. To complete the assessment, we evaluate how the hydrological response changes when using EO-C_m. Specifically, we replace L-C_m with EO-C_m and run the LISFLOOD model from 1990 to 2023, including two warm-up years (1990–1991). The remaining 13 model parameters are kept unchanged, allowing us to isolate the impact of C_m on river discharge and assess whether the current EFAS5 setup can realistically capture snow accumulation and melt dynamics in the selected catchments. These results are reported in Sec.4.3.

We compare the mean annual hydrograph of the two simulations, considering only the periods with available observations, to assess whether changes occur in SWE and snowmelt dynamics and whether these changes are reflected in the simulated discharge relative to observed river flows. In addition, we calculate the Kling-Gupta Efficiency (KGE) both over the entire period with observed river flows and on a monthly basis. This allows us to evaluate the overall performance of the simulations as well as their performance across different sections of the annual hydrograph, with particular attention to potential increases or decreases in performance during the snowmelt season. Finally we evaluate the spatial similarity of river discharge at pixel level to identify main difference between EO-C_m and L-C_m simulations upstream of the discharge station. The analysis focuses on upstream catchment areas larger than 100 km^2 to exclude very small headwater sections that may introduce noise in spatial comparisons. To do so, we extract daily river discharge time series from both model outputs and min-max normalized them for each grid cell location to standardize discharge values across different magnitudes and catchments. We then compute the Euclidean distance between the normalized discharge values of the two models at each grid cell, quantifying the absolute dissimilarity in flow dynamics over time. The Normalized Euclidean Distance (NED) values range from 0 to infinity, where a value of 0 indicates that the two time series are identical or highly similar, and larger values signify greater dissimilarity between the time series. These results are reported in Sec.4.4.

3 Test sites

In this study, we ~~analysed 9~~ analyze nine snow-dominated hydrological basins across Europe, located in Italy, Switzerland, Austria, Germany, France, Spain, Slovakia, and Sweden. These basins were selected for their strong snow influence on hydrological processes, with snow ~~cover~~ persisting for a significant portion of the year~~, and/or their particular climatic and morphological characteristics in relationship with snow processes~~. Representing a range of geographical contexts, ~~these basins encompass prominent mountainous regions like~~ the basins include mountainous regions such as the Alps and Pyrenees, as well as flatter terrains ~~such as those~~ in Scandinavia. ~~Additionally, these basins vary in land covercharacteristics, including different~~ They also exhibit diverse land cover, including varying proportions of forested areas, which ~~impact both~~ influence snow accumulation and melt~~dynamics.~~ .

For example, Mörrumsån ~~in Swedenand Laborec in Slovakiaare flat regions with briefand~~ (Sweden) and Laborec (Slovakia) are relatively flat with brief, intermittent snow periods~~. Laborec also exhibits~~ , with Laborec also having significant forest cover. Umeälven ~~in Sweden, though also relatively~~ (Sweden), though similarly flat, experiences prolonged snow cover lasting several months due to its high latitude. In contrast, the remaining basins ~~display~~ exhibit a more typical alpine snowpack. ~~Of the 9 catchments, 7~~ Some basins (Adige, Alpenrhein, Arve, and Salzach) contain glaciers, though glacier-covered areas are generally small —less than 1% of the total area (approximately 0.9% for Adige and Salzach, 0.6% for Alpenrhein)— with the exception of Arve, where glacierized areas account for about 5% of the basin. Two basins in Spain, Guadalfeo and Gállego, are strongly influenced by anthropogenic activities, providing an opportunity to assess model performance under different basin characteristics.

To further explore methodological differences, seven catchments were originally calibrated against observed river discharge, ~~whereas 2, the Guadalfeo and the Adige~~ while two—Guadalfeo and Adige—were parameterized using the regionalization approach ~~.~~ (see Sec. 2.2.1).

~~The availability of hydrological data was a constraint for the basin selection to ensure a complete analysis.~~ Key information on these basins is presented in Table 2 and Fig. 2. Due to the coarse model resolution, basin hypsometry is not accurately represented; for clarity, Table 2 reports the lower and upper bounds of elevation ranges used in the model, based on the three elevation zones described in Sec.2.2.2.

The EO dataset ~~covers six hydrological seasons~~spans six hydrological years, from October 1, 2017, to September 30, 2023, ~~i.e.,~~ corresponding to the period with maximum availability of Sentinel-2 data (both Sentinel-2A and Sentinel-2B). The LISFLOOD evaluation (see Sec. 4.4) covers a longer period (~~1992-2022) allowing to build a climatology. The grid of the model~~ 1992–2023) to allow a long-term analysis. The availability of hydrological data was an additional selection criterion to ensure a complete analysis. The analysis uses the model grid with a spatial resolution of ~~around~~ 1 arc-minute (~~approximately~~ ≈1.4 km)~~is considered for the analysis, as mentioned previously~~ , as described in Sec. ~~??~~2.2.

Table 2. Overview of the nine hydrological catchments selected in this study, including their respective countries, area, and elevation information. The mean elevations reported here refer to the elevation from the MERIT DEM aggregated at the model resolution of 1 arcmin. Maximum and minimum elevations are calculated considering σ_{topo}, thus representing the minimum and maximum elevations modelled.

Basin	Countries	Area [km^2]	Elevation [m]		
			min	mean	max
Adige	Italy	12100	3	1497	3724
Alpenrhein	Switzerland/Austria	7400	389	1660	3276
Arve	France	2000	344	1372	4413
Gállego	Spain	3900	199	798	2922
Guadalfeo	Spain	1200	70	1293	3294
Laborec	Slovakia	1300	136	421	980
Mörrumsån	Sweden	3500	9	186	310
Salzach	Germany/Austria	6700	348	1260	3295
Umeälven	Sweden	6100	318	711	1557

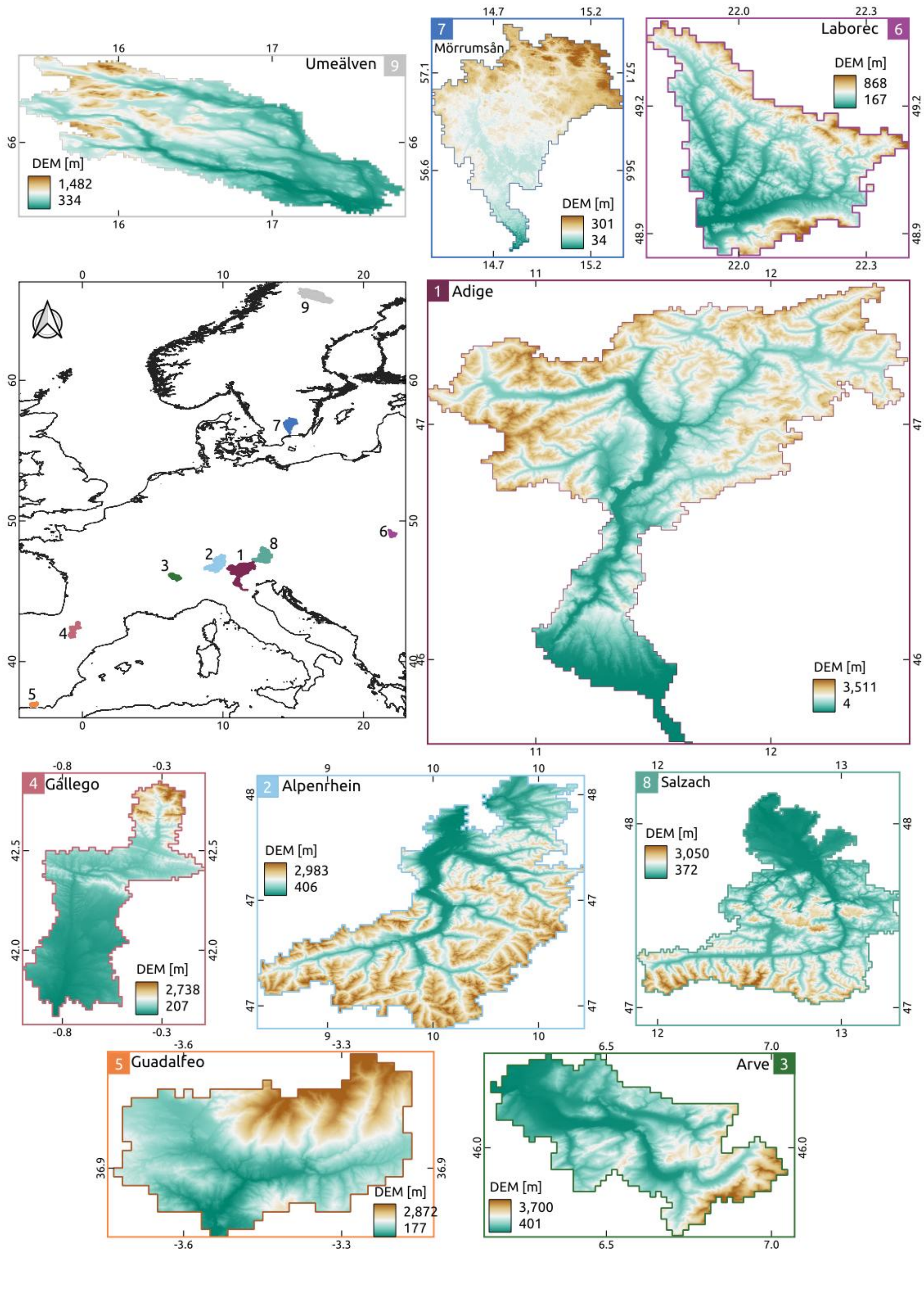

Figure 2. Overview of the nine hydrological basins chosen for this study: Adige (Italy), Alpenrhein (Switzerland/Austria), Arve (France), Gállego and Guadalfeo (Spain), Laborec (Slovakia), Mörrumsån (Sweden), Salzach (Germany/Austria) and Umeälven (Sweden). The elevations reported here (and hence the color bar ranges) refer to the MERIT DEM aggregated at the model resolution of 1 arcmin.

4 Results

4.1 Snowmelt Coefficient Calibration

In this section, the results of a dedicated calibration of the snowmelt coefficient we present the snowmelt coefficients (C_m using EO data) obtained by calibrating against EO data (EO-C_m - see Fig. 4), as described in Sec. 2.4, are reported. To differentiate between the snowmelt coefficient derived from traditional hydrological calibration and that obtained through EO data, we will refer to them as LISFLOOD C_m (L-C_m) and earth observation C_m (EO-C_m). Moreover, we also conducted a comparison of and compare them qualitatively with the coefficients obtained using the formula in Eq. C2 with those derived through the L-BFGS-B optimization. We refer to EO-$C_{m,1}$ and EO-$C_{m,2}$ to differentiate between the two approaches. Note that EO-$C_{m,1}$ and EO-$C_{m,2}$ are obtained as average values considering the first five hydrological years, while season 2022/23 is used as an independent dataset for evaluation purposes only.

In Figs. ?? and ??, the snowmelt coefficients from the EFAS5 calibration (L-C_m are shown together with the new coefficients EO-$C_{m,1}$ and EO-$C_{m,2}$ - see Fig. 3), as described in Sec. 2.2.1. The corresponding histograms are also illustratedshown in the figures. Missing values (in white color) correspond to masked areaswhite areas) indicate masked regions, such as water bodies , or pixels that never experienced snow for the analysed period. did not experience snow during the analyzed period.

Notable differences are evident between the three approaches, both in terms of spatial patterns and magnitude of the coefficients. Especially observed, as L-C_m represents a lumped coefficient, whereas EO-$C_{m,2}$ shows C_m is spatially distributed. EO-C_m exhibits very high values for in basins or areas where ephemeral snowis present. Note that with ephemeral snow. Additionally, the parameter range in the LISFLOOD calibration is narrower standard LISFLOOD calibration (2.5-6.5) –6.5) is narrower than in the EO calibrations. This larger range EO-based calibration. The wider range in EO-C_m allows us to evaluate explore the potential of the new calibration to correct compensate for erroneous precipitation inputs and better represent the melting snowmelt phase (see next section). It is interesting to note that the coefficient EO-C_m assumes a value of 10 in those basins, or parts of basins, that exhibit ephemeral or short snow-cover periods, such as the Laborec and Mörrumsån, as well as the lower Adige. This value likely indicates a non-ideal optimization, possibly due to fluctuations in snow cover. We also evaluated the stability of this coefficient across different seasons. For brevity, results are reported only for the Adige River basin in Fig. 5. The figure shows that the coefficient is quite stable over years, confirming our choice of considering a temporal average.

Snowmelt coefficients estimated using the hydrological calibration of LISFLOOD (L-C_m, on the left), EO data via Eq. C2 (EO-$C_{m,1}$, in the middle), and EO data through the optimization approach (EO-$C_{m,2}$, on the right). The corresponding histograms are also included. Missing values (in white) correspond to masked areas, such as water bodies, or pixels that never experienced snow for the analysed period.

To explore whether the spatialized snowmelt coefficient calibrated at the pixel scale captures meaningful patterns, we conducted a correlation analysis with topographic, geographic, and land cover features. The motivation was that such relationships could eventually support parameterizing snowmelt based on spatial characteristics alone, thereby reducing reliance on EO data, which are often labor-intensive to process. Table 3 reports the Pearson correlation coefficients between EO-C_m and several

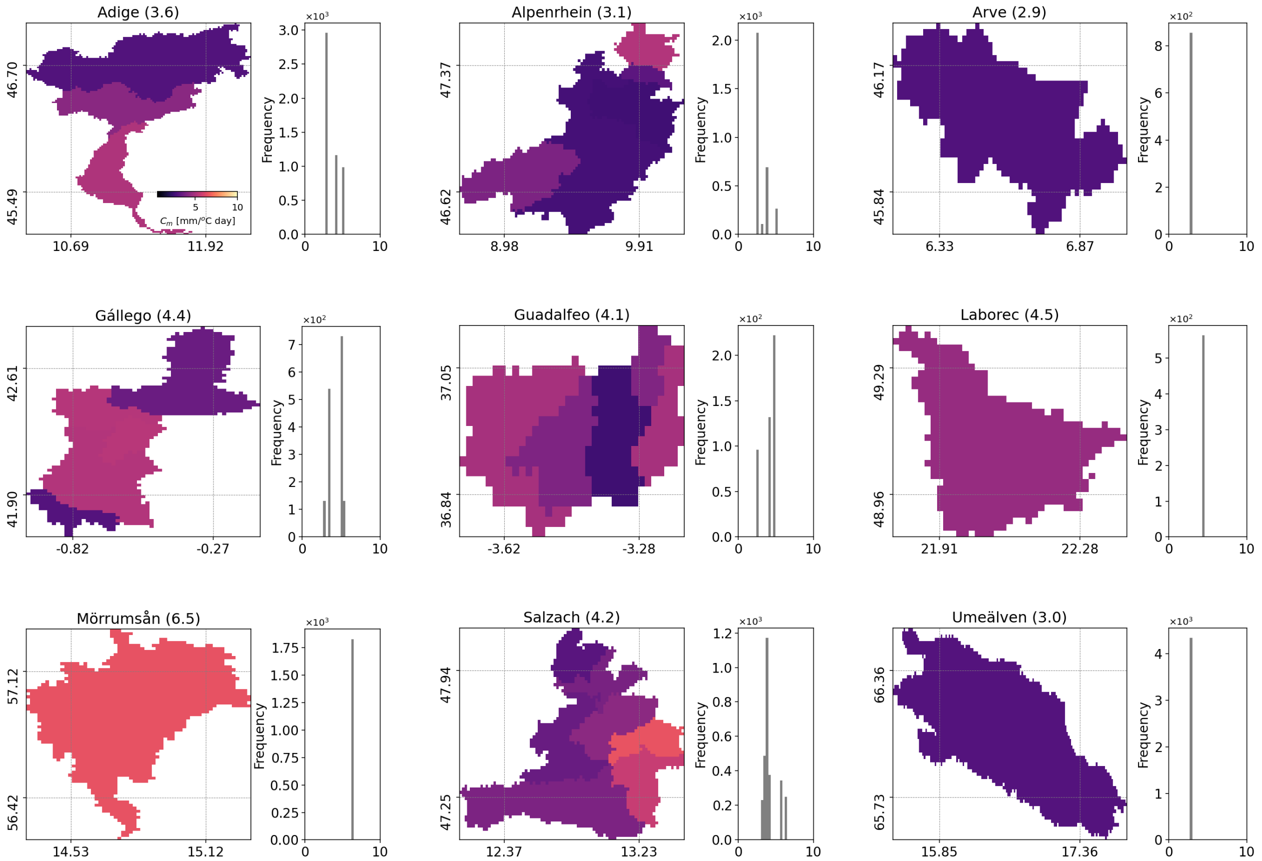

Figure 3. Snowmelt coefficients resulting from the standard hydrological calibration (L-C_m) for the nine selected basins. The corresponding histograms are also included. Missing values (in white) correspond to masked areas, such as water bodies, or pixels that never experienced snow for the analysed period. Average values are reported within brackets.

variables: elevation (DEM), elevation variability (DEM σ), slope, forest cover, mean snow cover duration (SCD), as well as mean precipitation (P) and temperature (T), averaged over the six analyzed hydrological seasons. However, the results indicate that no strong correlations emerge from this analysis. The most influential feature appears to be elevation, which exhibits a negative correlation in the Adige, Arve, Salzach, and Guadalfeo river basins. This indicates that lower values of EO-C_m are estimated for higher elevations, meaning snow persists longer at higher elevations, as expected. For the Laborec and Umeälven basins, which are relatively flat, the correlation with elevation becomes positive. The correlation with mean snow cover duration also aligns with the findings for elevation, confirming that snow lasts longer at higher elevations.

4.2 Snow Cover Evaluation

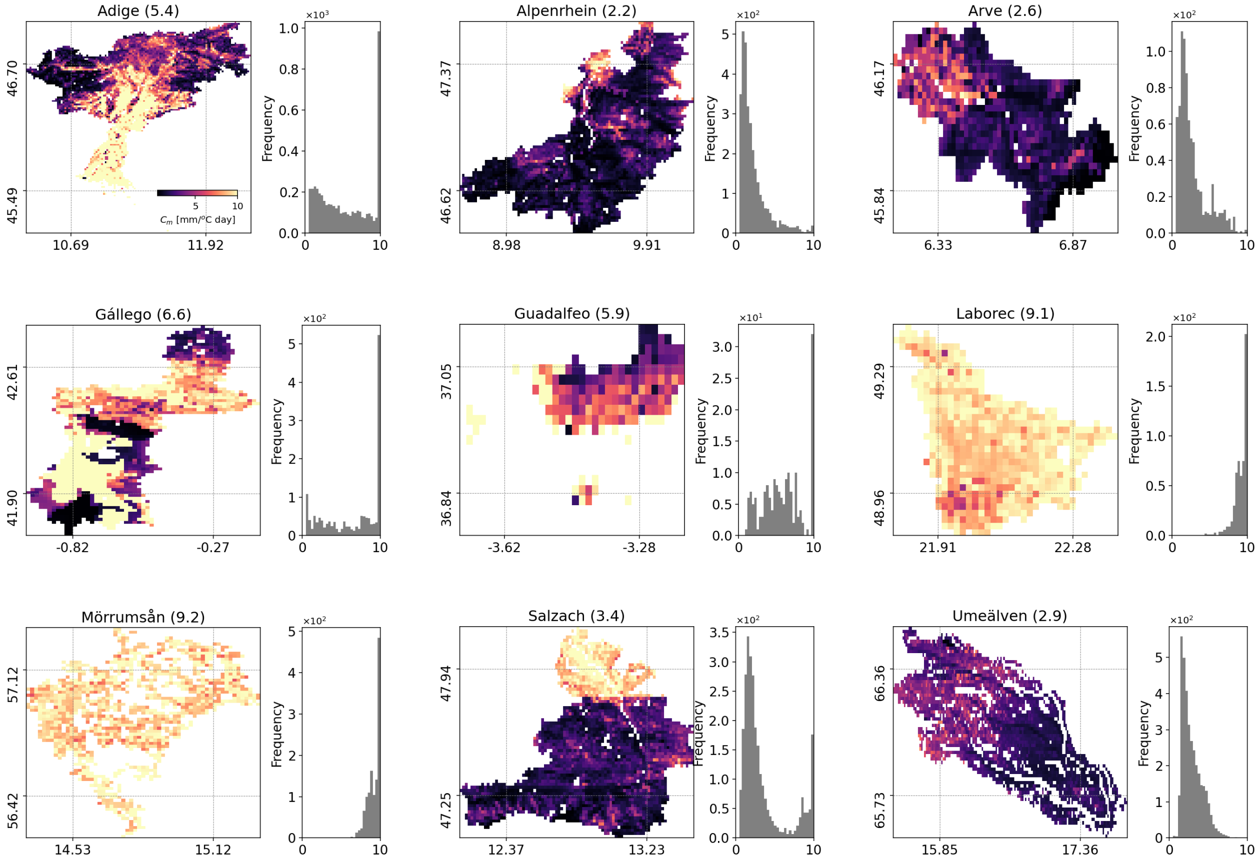

Figure 4. Snowmelt coefficients resulting from optimazion based calibration against earth observation SCF (EO-C_m) for the nine selected basins. The corresponding histograms are also included. Missing values (in white) correspond to masked areas, such as water bodies, or pixels that never experienced snow for the analysed period. Average values are reported within brackets.

Table 3. Pearson correlation coefficients between the EO-C_m and topographical, land cover and meteorological features.

	DEM	**DEM σ**	**Slope**	**Forest**	**SCD**	**P**	**T**
Adige	−0.58	−0.22	−0.05	0.52	−0.68	0.13	0.55
Alpenrhein	−0.29	−0.42	−0.16	−0.06	−0.36	0.31	0.18
Arve	−0.50	−0.48	−0.32	0.06	−0.54	−0.42	0.47
Gállego	−0.08	−0.05	−0.05	0.34	−0.28	−0.07	0.03
Guadalfeo	−0.77	−0.15	−0.06	0.65	−0.71	−0.36	0.72
Laborec	0.45	0.17	0.25	0.40	0.32	0.40	−0.48
Mörrumsån	−0.03	0.11	0.08	0.21	−0.08	−0.02	−0.04
Salzach	−0.55	−0.68	−0.39	−0.06	−0.68	−0.42	0.50
Umeälven	0.42	−0.03	0.08	−0.55	0.32	0.67	−0.34

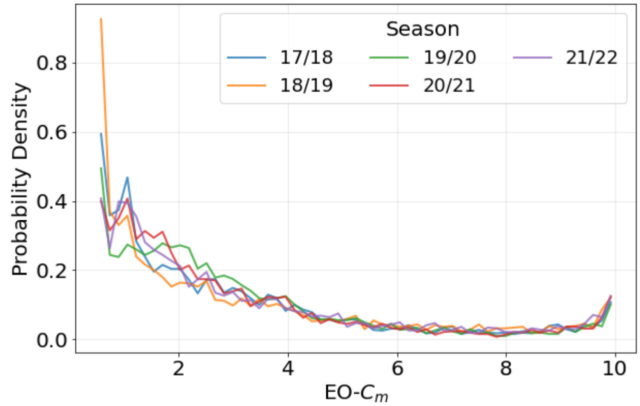

Figure 5. Snowmelt coefficients estimated using the hydrological calibration Probability density of LISFLOOD (L-C_m, on the left), EO data via Eq. C2 (EO-$C_{m,1}$, in the middle), and EO data through snowmelt coefficient for the optimization approach (EO-$C_{m,2}$, on Adige basin during the right)calibration season. The corresponding histograms Values of 10 are also included. Missing values (in white) correspond to masked areas, such as water bodies, or pixels that never experienced snow excluded for the analysed periodbetter visualization.

To test the newly estimated coefficients, we substituted them into Eq. 2 to calculate the updated SWE. Subsequently, we compared the EO-SCA with the SCA derived from the LISFLOOD model (L-SCA), considering the To assess how well the standard multi-parameter calibration of streamflow captures snow dynamics and to quantify the improvements of an independently calibrated C_m, we conducted a comparative evaluation of the snow cover area (SCA). Specifically, we ran the LISFLOOD snow module using two different snowmelt coefficients: the standard, lumped value (L-C_m, EO-$C_{m,1}$ and) and the new spatially-distributed value (EO-$C_{m,2}$$C_m$). This produced two distinct model-derived SCA estimates (L-SCA), which were then compared against the observed SCA (EO-SCA).

In Fig. 6, the SCA trends with different the two C_m are reported. Similarly, yearly scatterplots are provided in Fig. D1 in Appendix D. These results offer a quick overview of the performances at basin level. Furthermore, to assess improvements at the pixel-scale we report the metrics for SCF, using EO-SCF as the benchmark. These are computed per pixel along the temporal dimension and then averaged spatially. To specifically assess the model's ability to detect snow cover, we exclude pixels where both the target and reference SCF are 0 (snow-free). While including these pixels would lead to better performances, the results might be biased especially when a large portion of the basin is snow-free.

In Table 4, we present the average metrics calculated across all analysed hydrological seasons years for brevity. Similar metrics with a different SCF parametrization are reported in Table B1. Detailed metrics for each season individually are provided in Table D1 in Appendix D.

Due to variations in the size and location of these basins, the SCA varies significantly and exhibits seasonal fluctuations influenced by whether how wet or dry the year waswetter or drier. For example, while most basins reach nearly 100% snow cover at least briefly, others, such as Gállego and Guadalfeo, show very little snow cover. A generally good agreement can

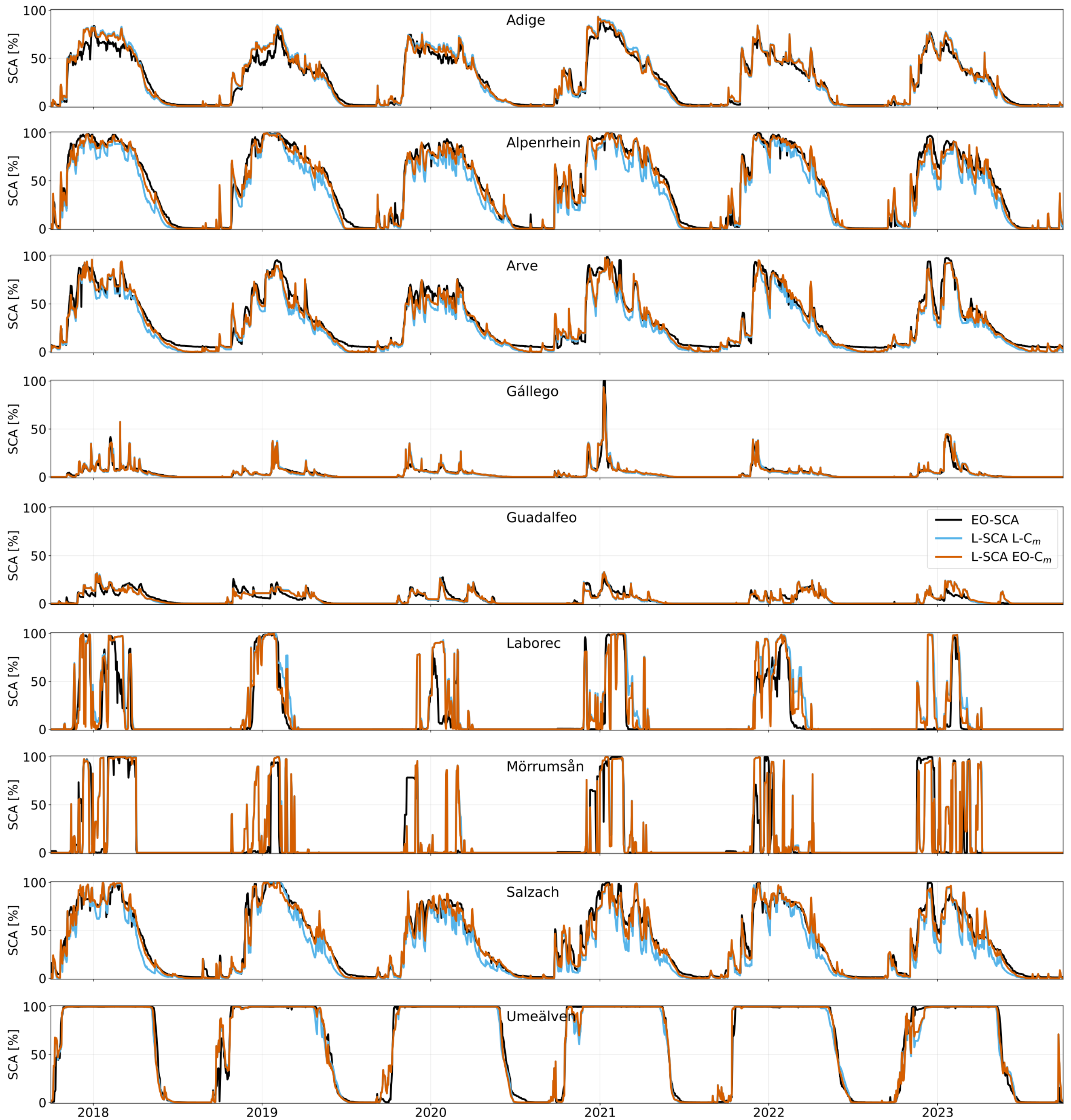

Figure 6. SCA trends for the nine river basins. In black, the observed EO-SCA, in ~~light blue~~ cyan the LISFLOOD ~~derived~~ simulated SCA ~~calculated with~~ using the standard EFAS5 snowmelt coefficient (L-C_m~~, in green the LISFLOOD SCA calculated with EO-$C_{m,1}$~~), and in orange the LISFLOOD ~~derived~~ simulated SCA ~~calculated with~~ using the EO-optimized coefficient (EO-~~$C_{m,2}$~~C_m).

Table 4. Evaluation of LISFLOOD SCF in terms of BIAS, RMSE, and correlation using the EO-SCF as ~~the~~ benchmark. The ~~three different~~ standard EFAS5 snowmelt ~~coefficients~~ coefficient (L-C_m~~, EO-$C_{m,1}$~~) and the EO-optimized coefficient (EO-~~$C_{m,2}$~~C_m) were utilized. Pixels where both the target and reference SCF are snow-free are excluded from the analysis.

	L-C_m			**EO-C_m**		
	Bias [%]	**RMSE [%]**	**ρ [-]**	**Bias [%]**	**RMSE [%]**	**ρ [-]**
Adige	9.86	35.76	0.61	8.11	32.60	0.62
Alpenrhein	−12.68	32.58	0.69	−4.99	24.56	0.75
Arve	−11.77	34.68	0.63	−6.33	30.32	0.65
Gállego	−0.63	44.31	0.52	−1.32	40.78	0.55
Guadalfeo	7.22	28.08	0.33	5.93	26.95	0.30
Laborec	22.43	48.81	0.46	14.67	46.39	0.46
Mörrumsån	6.95	54.58	0.27	5.29	54.50	0.27
Salzach	−6.96	36.89	0.67	−0.22	29.24	0.70
Umeälven	−1.21	20.46	0.59	−0.49	18.00	0.64

be observed between EO and LISFLOOD SCA, even ~~before applying the new coefficient~~with the EFAS5 calibration (L-C_m). However, important differences are evident in certain basins, including the Adige, Laborec, and Mörrumsån. In the Adige river basin, the LISFLOOD model shows a consistently larger SCA compared to satellite observations. These discrepancies, particularly noticeable during accumulation phases, such as in the 2020/21 season, may stem from an overestimation of snowfall and, consequently, precipitation fields over the basin, or from an inaccurate partition of solid/liquid precipitation. Despite these differences in magnitude, the timing of SCA variations appears to align well between the two datasets. Interestingly, the Arve basin ~~demonstrates that the SCA remains greater than 0 even during the summerseason~~shows that SCA remains above zero even during summer, as some pixels ~~persist as snow~~ are either persistently snow-covered or correspond to glacierized areas. ~~Notably, in the current setup of LISFLOOD~~ However, since LISFLOOD does not explicitly represent glaciers, these pixels ~~do not persist as snow, whereas correcting the coefficient results in a better representation~~are not simulated as permanently snow-covered in the model, thus resulting in lower SCA. On the other hand, the differences observed in the Laborec and Mörrumsån basins are more likely attributable to challenges in snow detection by the satellite. These include prolonged periods of missing acquisitions due to cloud cover, combined with ephemeral snowfalls in flat areas, as is the case in Mörrumsån. Additionally, significant forest coverage, particularly in the Laborec basin, further complicates accurate snow detection.

~~In general, all three approaches~~ Overall, both the standard EFAS5 calibration and the EO-based optimization of the snow module yield satisfactory results ~~when evaluated at~~ at the basin scale. However, important differences are highlighted when considering SCF (Table 4). Before dedicated EO-based calibration, the agreement is acceptable, with the highest bias observed at approximately 20% for the Laborec basin but with generally moderate correlation. The highest root mean square error (RMSE) values are observed for Mörrumsån and Laborec, due to the reasons previously discussed. Additionally, Gállego also exhibits notable discrepancies, likely because most pixels remain snow-covered for only short periods complicating the analysis. The computed metrics indicate that, in general, the optimization approach (EO-$C_{m,2}$$C_m$) improves bias, RMSE, and correlation, except for a slight increase in bias for Gállego. Conversely, EO-$C_{m,1}$ produces poorer results, often yielding higher bias and RMSE than L-C_m, except for Alpenrhein and Arve. As shown in Table D1, these trends generally persist across individual seasons, with a few exceptions. Additionally, for the year not used in coefficient calibration (2022/23), EO-$C_{m,2}$ C_m still demonstrates an overall improvement in performance especially in reducing the bias and RMSE and increasing the correlation. However, the remaining errors stem from the fact that the new coefficient enhances SCF during the melting season only, while errors persist during the accumulation season.

The poorer performance of We further investigate the dependency of model performance on catchment characteristics. Performance is evaluated in terms of BIAS (Fig. 7) and RMSE (Fig. 8) of SCF derived from EO-$C_{m,1}$ can be attributed to the fact that it is designed to perform well under conditions where a pixel remains continuously snow-covered, with well-defined snow accumulation and melting periods. However, as also stated by Pistocchi et al. (2017), this simplifying assumption may not hold in cases of intermittent snow coveror irregular snow dynamics. The presence of intermittent snow might also be attributed to errors present in the satellite-based product, particularly during the final melting phase when snow patches are present, leading to difficulties in applying the formulaC_m, and these metrics are compared against a set of physiographic features (mean elevation, forest coverage, and slope) and climatic features (mean precipitation, mean temperature, and snowfall). We also distinguish between glacierized and non-glacierized basins.

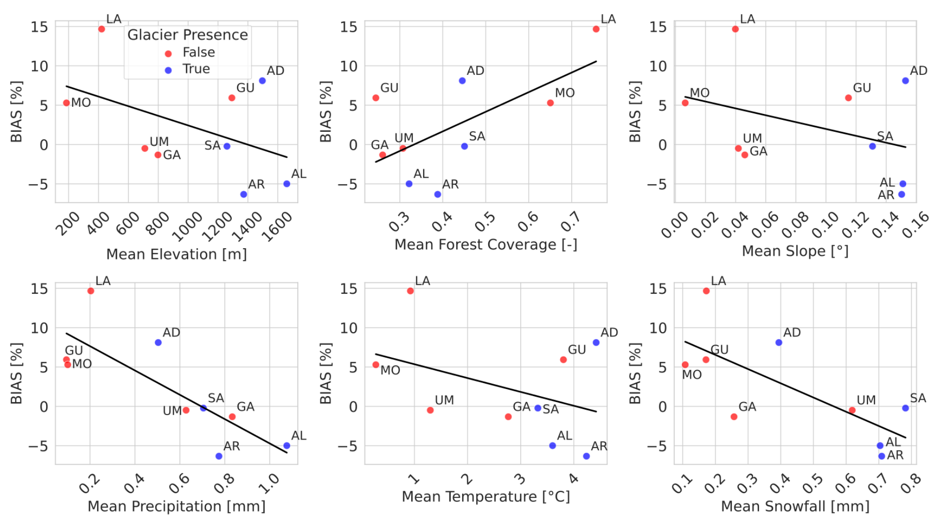

Figure 7. Bias of SCF obtained using EO-C_m in relation to selected physiographic and climatic features. Basin identifiers are indicated by their initial letters. Glacierized basins are marked in blue, and non-glacierized basins in red.

The analysis shows that errors tend to be larger in lower-elevation and flatter catchments, with a similar increase associated with higher forest coverage. For the climatic features, we find an inverse relationship with RMSE: basins characterized by higher precipitation and snowfall generally exhibit lower errors. This aligns with expectations, as lower precipitation—particularly

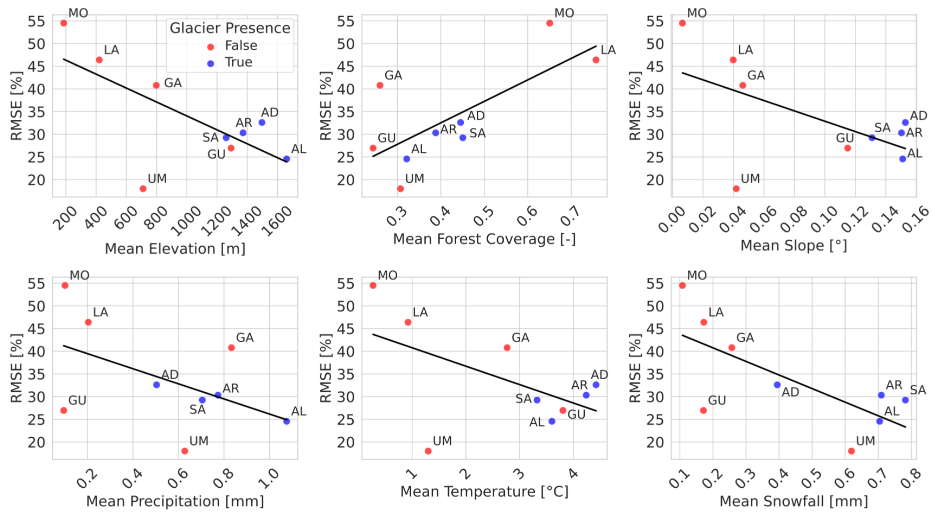

Figure 8. Root mean square error of SCF obtained using EO-C_m in relation to selected physiographic and climatic features. Basin identifiers are indicated by their initial letters. Glacierized basins are marked in blue, and non-glacierized basins in red.

in the form of snowfall—typically results in more ephemeral snow cover, increasing the prevalence of fractional snow-covered areas, which are more prone to both detection and modeling errors. Glacierized catchments do not, on average, display substantially different performance relative to non-glacierized ones. The Umeälven basin always shows markedly lower RMSE. This is likely due to its prolonged and near-complete seasonal snow cover, which reduces snow-cover variability and associated modeling errors.

It is also interesting to analyse the monthly evolution of bias and RMSE, as shown in Fig. 9. Overall, model performance tends to deteriorate during the summer months across all basins, reflecting the snow depletion phase. This reduction in performance is partly driven by the smaller number of snow-covered pixels considered (snow-free pixels are excluded), which are often characterized by fractional snow cover and thus more prone to errors. Nevertheless, despite this seasonal decline, we generally observe an improvement when applying EO-C_m.

4.3 ~~Effects on~~ Snow Water ~~Balance~~Equivalent Intercomparison

To fully assess the performance of the ~~new melting coefficient in improving water balance estimates~~snow module before and after snow melt coefficient recalibration, spatialized SWE maps would ideally serve as a reference. However, a comprehensive analysis is not feasible due to significant challenges in data availability and usability. Given the spatial resolution of a LISFLOOD pixel, in-situ measurements are unreliable proxies, as they fail to capture intra-pixel variability — particularly in basins with complex topography. Additionally, SWE data is often missing, and when only snow height measurements are available, converting them to SWE requires assumptions about snow density, introducing further uncertainty. Remote sensing products also have limitations. The accuracy of SWE derived from microwave sensors is affected by factors such as vegetation

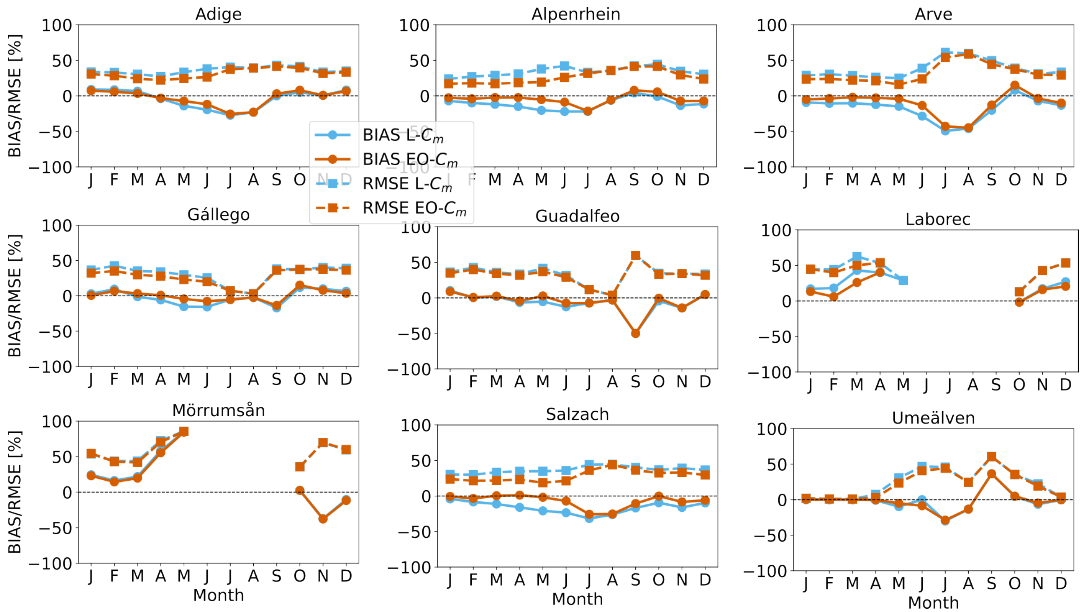

Figure 9. Monthly BIAS and RMSE trends for the nine river basins. In cyan, the BIAS (solid line marked with dots) and RMSE (dashed line marked with squares) calculated by using L-C_m. In orange, the same calculated with EO-C_m.

cover, topography, and snow type (Pulliainen et al., 2020). Furthermore, many available datasets, including those from the Copernicus Land Monitoring Service, have coarse spatial resolutions and often exclude ~~mountainous~~ mountain areas, further restricting their applicability (Takala et al., 2011). Therefore, we propose an intercomparison with SWE estimates from two ~~additional~~ different models in the Adige and in a subchatchment of the Alpenrhein, ~~along with an analysis based on monthly climatology in terms of LISFLOOD outputs for all the catchments.~~

~~Regarding the SWE intercomparison, we considered~~ the Dischma Valley. For the Adige, we consider the IT-SNOW reanalysis dataset ~~for the Adige basin~~ (Avanzi et al., 2024) (see Fig. 10). ~~Additionally, for a small sub-basin of the Alpenrhein, the DischmaValley~~For Dischma, we compare our results with the Swiss Operational Snow-Hydrological (OSHD) model system, available for the ~~for the~~ first five seasons (Mott, 2023; Mott et al., 2023) (see Fig. 11). The metrics are reported in Table 5.

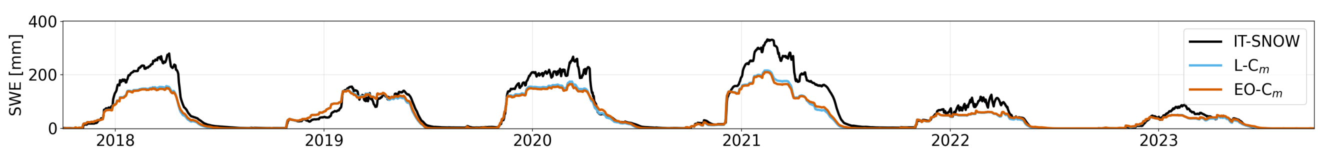

Figure 10. SWE time-series for the Adige river basin. In black the ~~SWE~~ simulation from ~~the~~ IT-SNOW~~model~~, in cyan the ~~SWE obtained with~~ LISFLOOD simulation using the standard EFAS5 snowmelt coefficient (L-~~C_m~~C_m), ~~in green the SWE obtained with EO-$C_{m,1}$~~ and in orange the ~~SWE obtained with~~ LISFLOOD simulation using the EO-optimized coefficient (EO-~~$C_{m,2}$~~C_m).

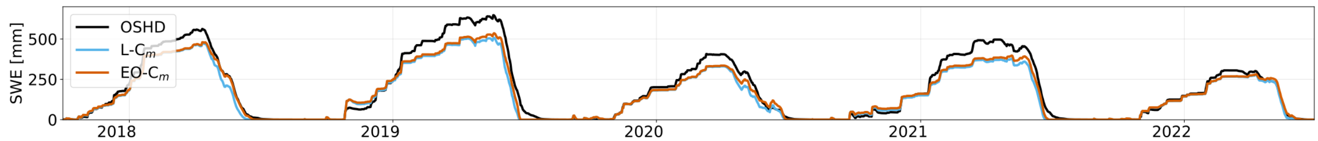

Figure 11. SWE time-series for the Dischma ~~valley belonging to the~~ (Alpenrhein~~river basin~~). In black the ~~SWE~~ simulation from ~~the~~ OSHD~~model~~, in cyan the ~~SWE obtained with~~ LISFLOOD simulation using the standard EFAS5 snowmelt coefficient (L-~~C_m~~C_m), ~~in green the SWE obtained with EO-$C_{m,1}$~~ and in orange the ~~SWE obtained with~~ LISFLOOD simulation using the EO-optimized coefficient (EO-~~$C_{m,2}$~~C_m).

Table 5. Evaluation of LISFLOOD SWE in terms of BIAS, RMSE, and correlation using IT-SNOW as the benchmark for Adige and OSHD for Dischma (Alpenrhein). The ~~three~~ two different snowmelt coefficients L-C_m, EO-~~$C_{m,1}$ and EO-$C_{m,2}$~~ C_m were utilized. Pixels where both the target and reference SCF are snow-free are excluded from the analysis.

	L-C_m			**EO-C_m**		
	Bias [mm]	**RMSE [mm]**	**ρ [-]**	**Bias [mm]**	**RMSE [mm]**	**ρ [-]**
Adige	−53.54	106.40	0.44	−56.32	106.82	0.43
Dischma (Alpenrhein)	−38.10	80.60	0.96	−26.93	79.63	0.96

The results confirm a generally good agreement but also highlight LISFLOOD's tendency to underestimate SWE compared to the other models in both basins. These differences are most likely linked to discrepancies in precipitation input data. Notably, IT-SNOW assimilates snow height measurements, which can enhance the accuracy of accumulation estimates. ~~The SWE obtained with EO-$C_{m,2}$ falls between L-C_m and EO-$C_{m,1}$. Especially~~ Discrepancies in the input forcings might explain the general low correlation for the Adige (0.44/0.43), while for Dischma we obtain a very high correlation (0.96) both previous and after C_m replacement. Notably, especially for the Dischma Valley ~~,~~ the depletion curve is better captured when using ~~the new coefficient. Despite a lower bias obtained with~~ EO-~~$C_{m,1}$ for Dischma, RMSE and correlation are improved with~~ C_m. However, for both basins we obtain comparable or slightly improved metrics aligning with expectations based on the SCA comparison. Interestingly, we did not observe worse performance in representing different conditions, such as snow drought events, which appear to be reasonably well reproduced by both the standard and EO-~~$C_{m,2}$, which also appears to better represent the snow depletion by looking at the SWE trends. This aligns with expectations based on the SCA comparison~~C_m. This is particularly evident in the Adige basin during the 2021/22 and 2022/23 seasons. It should be noted that this analysis is not exhaustive, as it relies solely on intercomparison with other models ~~and~~ with inherent limitations stemming from model parameterizations and the quality of forcing inputs. Therefore, the analysis lacks validation against reference data.

~~To complete the assessment, we evaluated the changes in hydrological response resulting from the new coefficient . Since the optimization method generally provided better results, we conducted this analysis using~~

4.4 Effects on Long-Term LISFLOOD Simulations

In this section, we evaluate the hydrological response to post-replacement of the snowmelt coefficient (EO-~~$C_{m,2}$ only and compared it with~~ C_m), with results compared against benchmark simulations using the standard L-C_m. ~~For this purpose, the LISFLOOD model was run from 1990 to 2022, with 2 warm-up years (1990-1991~~Note that, as explained in Sec. 2.2.1, all the other parameters are kept unchanged, following EFAS5. Results are shown as daily averages calculated only for periods with available observations (Fig. 12). ~~The results are presented as monthly climatology between 1992 and 2022, derived from the monthly averages of the original 6-hourly model outputs 12. The outputs~~ Reported variables include SWE, snowmelt, ~~total runoff,~~ and discharge, all expressed in mm/~~month. The discharge climatology was calculated based solely on the dates with available observed data~~day. Dashed lines ~~represent~~ in the figure denote the 10th and 90th percentiles of the time series, indicating variability in the modeled hydrological response.

In most ~~of the~~ catchments, the new ~~snowmelt coefficient~~ EO-C_m ~~influences~~ affects the timing of ~~snow~~ both accumulation and melting phases, which ~~is,~~ in some cases ~~, reflected in~~ also influences the timing and magnitude of ~~total~~ runoff. In the Adige basin, the ~~snow cover behavior is similar across~~ behavior of the snow cover is similar in both runs. ~~However,~~ The benchmark has a higher peak in SWE in March, but a higher depletion as well from April onward. This is reflected in the snowmelt, where the EO-run shows a slight shift in the timing of snowmelt, with ~~its peak occurring in May~~ lower snowmelt between March and May and higher in June, compared to ~~the benchmark run where the peak is more evenly distributed between April and May~~EFAS5. This shift has minimal impact on the generation of ~~total runoff~~discharge. Notably, the snowmelt coefficient assigned through the regionalization approach aligns closely with that derived from the EO-SCA.

In the Alpenrhein, ~~Arve,~~ Gállego and Salzach basins, the new EO-runs show an increase in snow accumulation, driven by reduced snowmelt before the peak. This results in a higher magnitude of snowmelt and a shift in its timing, with the peak occurring later compared to the benchmark. The effect of the newly calibrated snowmelt coefficient extends to ~~runoff generation~~discharge, leading to increased ~~runoff~~ discharge during the snowmelt phase and reduced ~~runoff~~ discharge during the snow accumulation phase. This shift does not affect the daily average discharge in the Gállego basin, but it does influence the Alpenrhein River, where it improves the agreement with observations during July and August. In case of Salzach basin the increased discharge between June and July is overestimating the observed discharge, with EFAS5 having a better match with observations.

The EO-run of the Arve basin shows a positive bias in SWE, which is only partially reflected in snowmelt since more SWE does not melt during the summer period. Snowmelt is significantly higher between June and August, and matching better observed river discharge for the same period.

In the Guadalfeo basin, a slight decrease in the snowmelt peak is observed, occurring in March, with no impact on total runoff. The model heavily underestimates river discharge compared to observations~~, the poor performance could be partially explained by the regionalization assignment of the parameters~~. This poor performance may be partly due to the regionalization of parameter assignment and/or ~~by the fact that~~ the inclusion of the Rules reservoir ~~was opened in 2004, whereas is it has been included~~ in the model for the ~~whole~~ entire simulation period (~~1992-2022). Therefore, the observed climatology considers~~

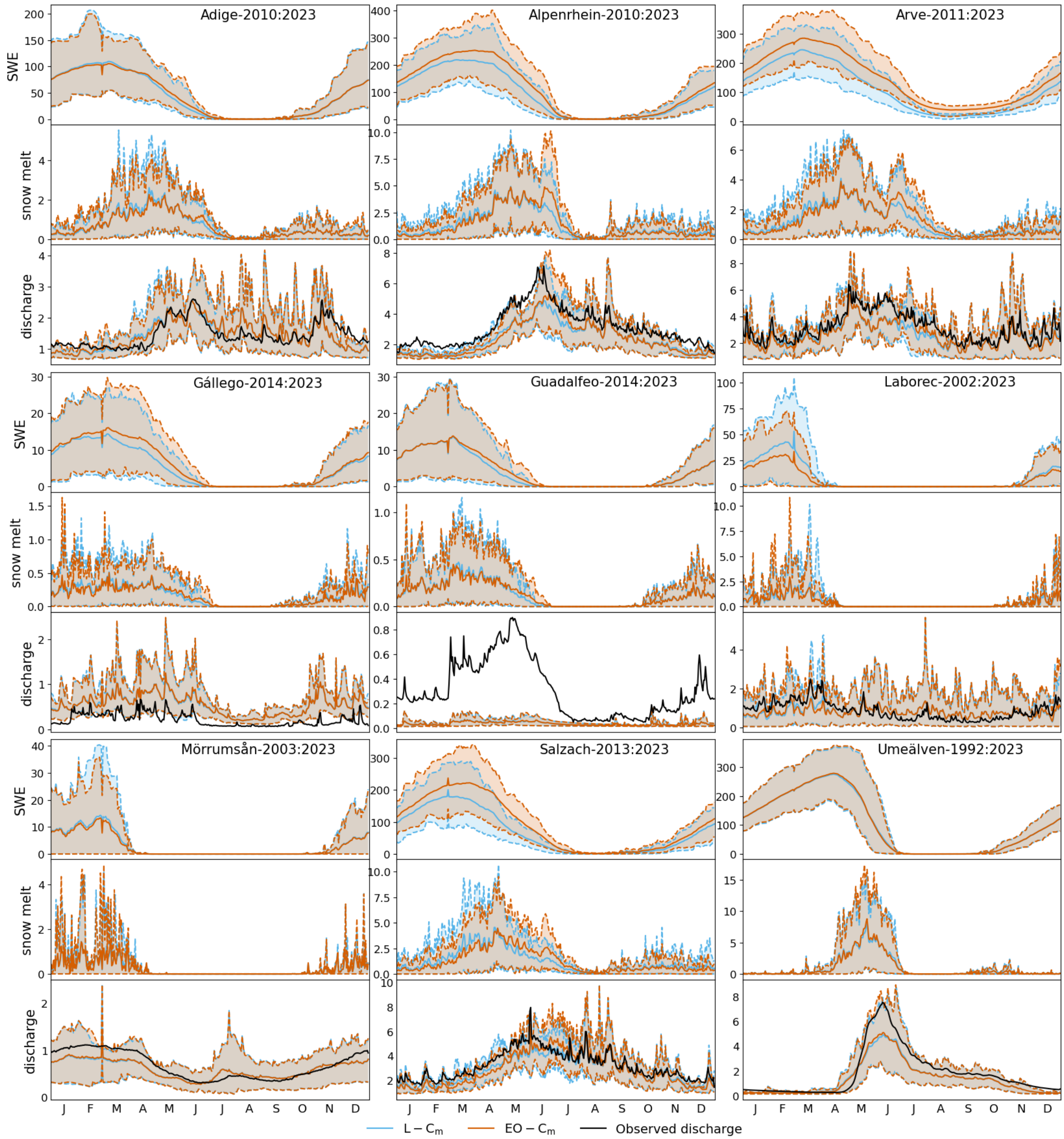

Figure 12. ~~Monthly climatology~~ Daily averages of SWE, snowmelt ~~, total runoff~~ and discharge, in mm/~~month~~day. In black, the ~~climatology~~ daily averages of observed river discharge, in ~~blue~~ cyan the benchmark run calculated using L-C_m, and in orange the ~~climatology~~ daily averages from the run with the new calibrated coefficient EO-C_m.

1992–2023), despite it was opened in 2004. The observed mean daily values account for 13 years ~~in which the reservoir didn't exist,~~ when the reservoir did not yet exist, as it was commissioned in 2004, whereas the simulation ~~considers that the reservoir was always there~~assumes the reservoir has been present throughout the entire period. In the Laborec basin, snow cover is reduced and snowmelt occurs earlier, peaking in February. Extreme values are reduced, with the 90th percentile decreasing from 60 to 52 mm for snow cover and from 100 to 80 mm/month for snowmelt. The ~~total runoff~~ discharge increases in January and February but decreases in March. While the flow regime is broadly similar to observations, notable differences remain with observed runoff being 30% higher than both simulations. In the Swedish catchments ~~,~~ Mörrumsån and Umeälven, no significant differences ~~in climatology are observed.~~ were found in mean daily values. The only noticeable deviation occurred in the 90th percentile of SWE in Mörrumsån, reflecting a period of high snow accumulation, followed by a sharp drop in SWE and increased snowmelt, likely driven by a temperature spike.

~~Performance statistics were computed using daily simulated and observed river discharge. Overall, the KGE values are similar between the two runs. However, slight~~ The performance statistic KGE, for the period with available observations, is reported in Tab. 6. Since the EO-C_m model was not recalibrated, a general decline in KGE and related metrics was expected. However, in most cases, the differences in metrics are not significant, and in some instances, there are improvements, which are highlighted in bold in Table 6. Across all catchments, the bias component remains virtually identical between the EO-C_m and L-C_m experiments, indicating that incorporating EO-C_m does not systematically increase or decrease the total volume of simulated discharge. A slight degradation is observed in correlation, particularly in the Laborec basin, suggesting that EO-C_m somewhat reduces the accuracy in capturing the timing of peak flows. This is particularly important in the operational context of EFAS5, where changes in correlation directly impact the system's ability to anticipate or delay peak flows. The impact on variability is more heterogeneous: improvements are observed ~~for the Adigeand Mörrumsån river~~ in the Adige, Guadalfeo, and Umeälven basins, while ~~KGE values for the Salzach , Laborec, and Alpenrheinriver basins have decreased.~~ reductions occur in the Salzach and Alpenrhein. This pattern implies that EO-C_m can have a positive effect on representing interannual flow fluctuations in some basins, but not universally. Overall, model performance increases in the Adige and Mörrumsån basins following the introduction of EO-C_m, whereas noticeable declines occur in the Alpenrhein, Laborec, and Salzach.

Fig. 13 presents monthly Kling-Gupta Efficiency (KGE) values for both EO-C_m (cyan) and L-C_m (orange) LISFLOOD runs. In most basins, such as Adige, Alpenrhein, Arve, Mörrumsån, and Salzach, both experiments achieve consistently high KGE scores (generally above 0.5), indicating robust model performance throughout the year. Conversely, in basins such as Gállego, Guadalfeo, and Umeälven, the simulations exhibit lower and more variable KGE scores, with several months showing negative values; this suggests poor performance and notable mismatches between simulated and observed river flows. The Gállego and the Guadalfeo basins in particular exhibit poor KGE in most months, which is reflected in their negative KGE in table 6; the EO-C_m did not yield significant improvements/worsening in these catchments. Performance differences between the two experiments are most pronounced in specific seasons. The EO-C_m model run outperforms the L-C_m run in the melting season of Arve and Alpenhrein, as well as in the snow accumulation season of the Adige and Mörrumsån basins. A decreased performance is observed for most months in the Salzach basin, while Laborec shows mixed results, with slight improvement in December and January and a decline in March and April.

~~Hydrological performance of current LISFLOOD configuration (benchmark) and LISFLOOD run with the new snowmelt coefficient~~

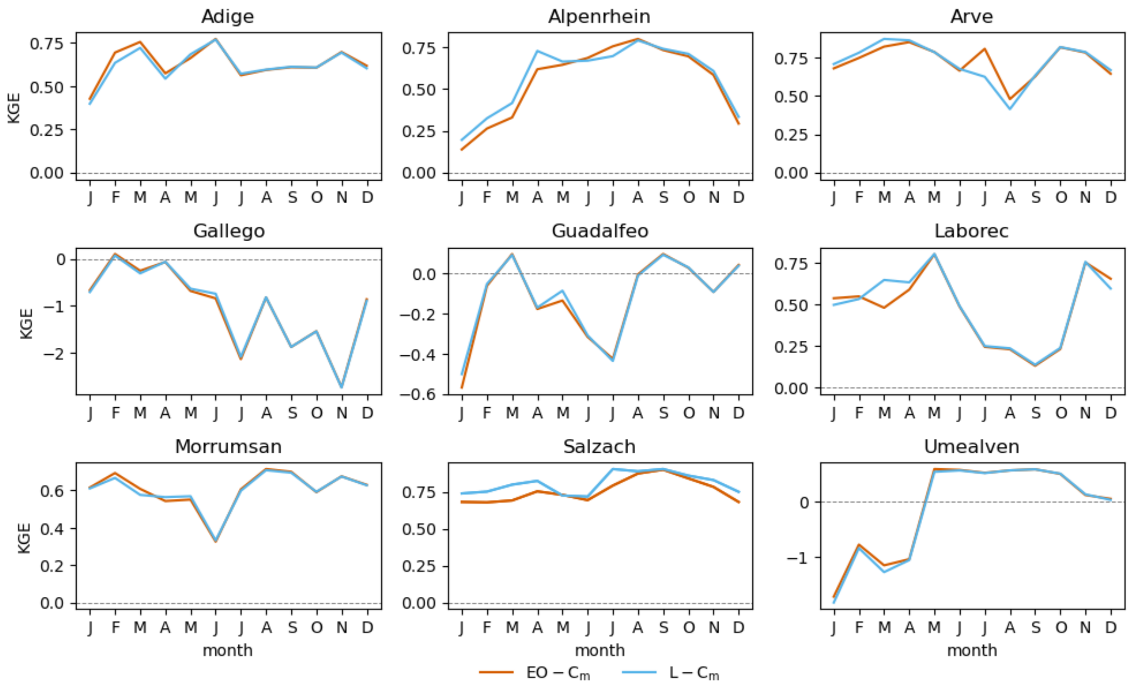

Figure 13. Monthly KGE calculated for both LISFLOOD runs against observed discharge. In cyan the benchmark run calculated using L-C_m, and in orange the run with the new calibrated coefficient EO-C_m.

Table 6. Hydrological performance of current LISFLOOD configuration (EFAS5) and LISFLOOD run with the new snowmelt coefficient. Together with the KGE, the bias ratio (β), the Pearson correlation (r) and the variability ratio (γ) are reported. In bold values with metrics that perform better using the EO-C_m snowmelt coefficient compared to EFAS5

	L-C_m				**EO-C_m**			
	KGE [-]	**β [-]**	**r [-]**	**γ [-]**	**KGE [-]**	**β [-]**	**r [-]**	**γ [-]**
Adige	0.75	0.96	0.76	1.04	**0.76**	**0.97**	0.76	**1.03**
Alpenrhein	0.73	0.75	0.90	1.01	0.70	0.75	0.89	1.12
Arve	0.80	0.83	0.89	0.99	0.80	0.83	0.89	0.99
Gallego	−0.50	2.37	0.77	0.45	−0.50	2.37	0.77	0.45
Guadalfeo	−0.08	0.10	0.55	0.61	−0.08	0.10	0.53	**0.63**
Laborec	0.74	0.98	0.75	0.93	0.69	0.98	0.70	0.93
Morrumsan	0.76	0.87	0.81	0.98	**0.77**	0.87	0.81	0.98
Salzach	0.85	0.88	0.91	1.00	0.82	0.88	0.89	1.07
Umealven	0.70	0.73	0.87	0.96	0.70	0.73	0.88	**0.98**

5 Discussion

In this study, we evaluated the LISFLOOD snow module and compared its current setup — which relies on traditional hydrological calibration to fine-tune the snowmelt coefficient — with two alternative approaches that use dedicated calibration to match satellite-derived snow cover data. Our findings reveal significant differences in the spatial distribution and magnitude of C_m across the different calibration approaches. Notably, LISFLOOD already produces reasonable SCA and SWE, particularly when assessed at the basin level. However, calibrating the snowmelt coefficient separately leads to improvements, especially in the representation of fractional snow cover and the depletion. Despite the substantial variations in the calibrated coefficients, the LISFLOOD snow module demonstrates low sensitivity to these changes when evaluated in terms of climatology of the water balance at catchmentscaleFig. 14 presents the NED for each catchment. Darker colors indicate river sections where the two models produce similar daily discharge (low NED), while lighter colors highlight areas of stronger divergence.

As expected, the optimization approach, which minimizes the error between the L-SCF and EO-SCF, yields more consistent snow cover. It significantly improves the agreement between the L-SCF and EO-SCF, overcoming challenges posed by the lack of continuous snow periods that might arise in the approach of Pistocchi et al. (2017). Notably, the optimized coefficient improves

The spatially heterogeneous EO-C_m shows a marked local impact in some river reaches with small upstream areas, where differences between model outputs are more evident. This influence decreases progressively downstream as localized effects are smoothed along the flow path. By the time discharge reaches the calibration points, typically located further downstream, the impact becomes negligible, as the calibration process compensates for or overrides local parameter variations. The Gállego and Mörrumsån basins exhibit the least effect from the EO-C_m implementation, with maximum NED values reaching only 1. Laborec and Umeälven follow, displaying peak NED values up to 3. In the remaining basins, most river reaches have NED values below 4, although some specific sections show higher localized NED values.

Reservoirs generally have minimal effect on the differences between the two simulated discharges across most basins. However, in the Gállego and Adige basins, distinct impacts are observed at the outflow of a single reservoir in each basin: in Adige, this occurs at the first upstream reservoir in the north-west area; in the Gállego, at the second reservoir moving downstream from the headwaters. In both cases, the grid cell immediately downstream of the reservoir shows greater differences than the grid cell directly upstream.

5 Discussion

This study tested whether replacing the LISFLOOD snowmelt coefficient with EO-calibrated values after a standard streamflow calibration can improve snow cover representation. The approach enhances realism without needing a full, time-consuming model recalibration. We would like to provide here a discussion on the outcomes and limitations of this study.

In its current EFAS5 setup, LISFLOOD already provides reasonable basin-scale estimates of SCA and SWE. However, optimizing the snowmelt coefficient with EO data improves the representation of SCF during the depletion phase, as C_m optimization reduces discrepancies between modeled and observed SCF. This enhances the consistency of the melting phase

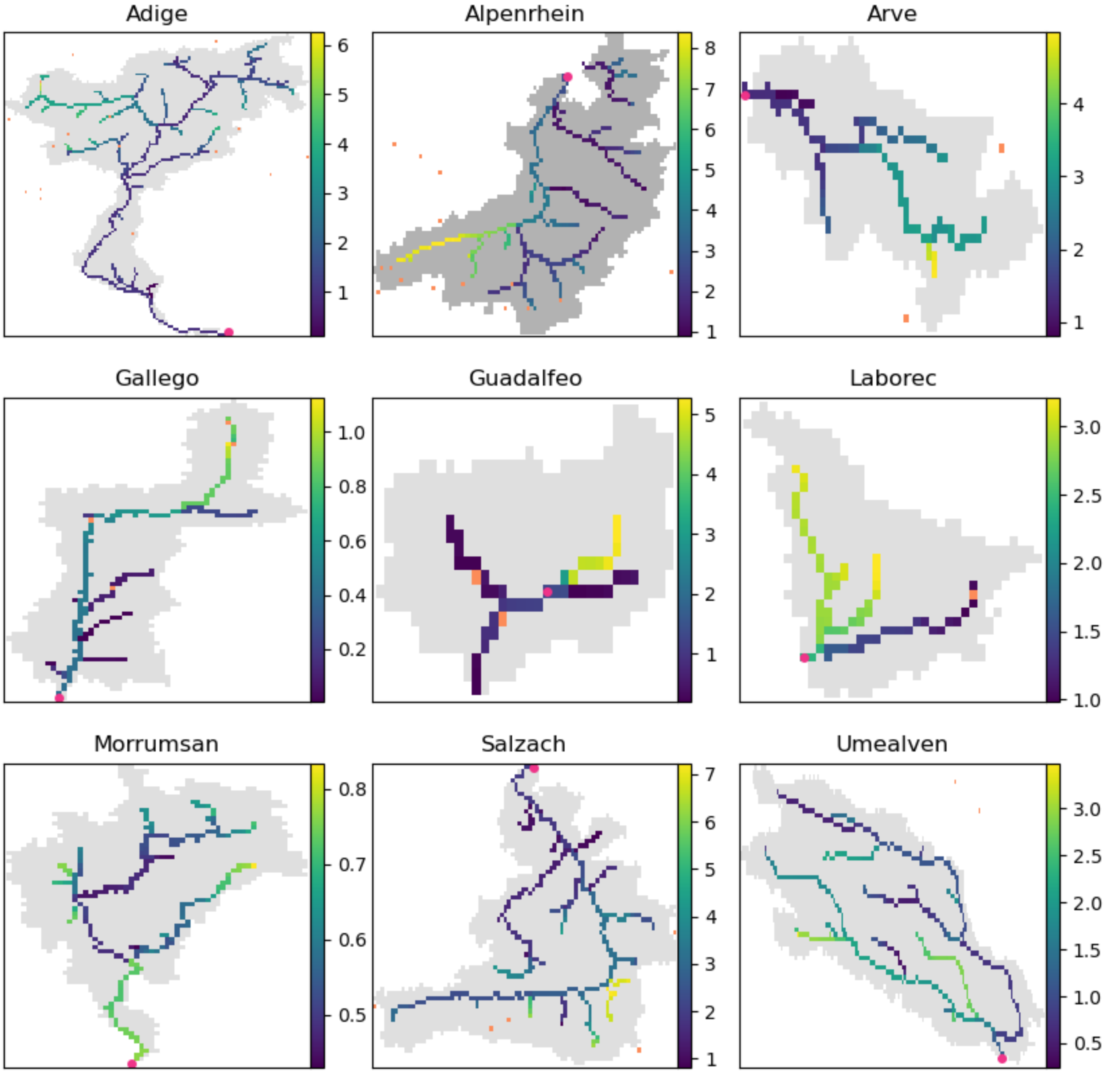

Figure 14. Normalized Euclidean Distance between daily discharge of LISFLOOD model as per in EFAS5 and the LISFLOOD model run with the EO-C_m coefficient. Light colors mean that the discharge are different, dark colors mean that discharges are similar. Reservoirs are highlighted in orange in the figure.

with ~~the depletion trends observed by the satellite, as shown in~~ satellite-observed depletion trends (Fig. 6~~. This effect is particularly evident in~~), particularly in basins such as the Alpenrhein, Arve, and Salzach~~river basins~~, where a ~~more linear snow season — characterized by a singleaccumulation and melting phase — likely facilitates better alignment. Basins where ephemeral snow is more frequent as~~ single, well-defined accumulation–melt cycle facilitates alignment. In contrast, basins with ephemeral snow cover, such as the Laborec and Mörrumsån~~show worse performances. However, it is important to discuss the reasons for further error sources.~~

~~A detailed analysis of the results indicates that these inconsistencies are primarily due to~~ , show poorer performance. Additional uncertainties also stem from limitations in the EO product itself: persistent cloud cover ~~in the satellite product, which~~ can lead to ~~reconstruction errors and inaccurate detection of snow cover. Additionally, forest coverage poses a significant challenge for snow detection using optical data, as optical sensors are unable to~~ errors in SCF reconstruction, while forested areas remain problematic for optical sensors that cannot detect snow beneath the canopy.

~~Discrepancies~~ We acknowledge also limitations linked to the LISFLOOD model. First, it operates at a coarse spatial resolution, which may not adequately capture processes in regions with complex topography. This choice is inherent to its role as a large-scale, operational model. Furthermore, the snow module is relatively simple and does not include glaciers. In this work, the accumulation scheme was not recalibrated, and key parameters, e.g., the temperature threshold for rain–snow partitioning, were not adjusted, even though they strongly influence snowpack evolution. As a result, errors introduced during the accumulation phase ~~are likely due to inconsistencies in the input forcings, particularly in the estimation of solid precipitation . Note that the optimization process does not affect the accumulation phase, as SWE is independent of the melting coefficient for those days~~remain uncompensated in the calibration. Uncertainties in the forcing inputs, particularly biases in precipitation, are likely a dominant source of error, affecting snow accumulation regardless of model parameterization. Improving precipitation datasets and explicitly calibrating accumulation-related parameters would likely enhance snow process representation in LISFLOOD. However, we emphasize that SCF data alone may not be sufficient to constrain the accumulation process, since precipitation events occurring over already snow-covered areas do not change SCF. While SCF is valuable for constraining depletion, additional approaches would be required for a more robust calibration of accumulation processes. Additionally, challenges in the SCF parameterization also contribute to ~~these discrepancies~~possible inaccuracies, as accurately converting SWE to SCF remains a complex issue.

Furthermore, assuming a constant snowmelt coefficient over time may be an overly strong assumption. Although our analysis in Sec. 4.1 showed an overall stability of the EO-C_m distribution across different seasons — and demonstrated that both EFAS5 and the new coefficient were capable of reproducing a range of conditions, from wetter seasons to snow-drought periods — variations in snow density, shallow snowpacks, or the presence of wind crusts, among others, can significantly affect snowmelt dynamics. While seasonality is accounted for through the addition of C_{seas}, this might not fully capture variations in snowpack characteristics. The sinusoidal function that defines C_{seas} merely adds a value in the range of ~~$\pm 0.5\ mm/C^{\circ} \cdot day$~~$\pm 0.5 \frac{mm}{°C \cdot day}$, without considering key geographical factors such as latitude, altitude, or aspect, which influence snowmelt. ~~Factors such as differences in snow density, shallow snowpacks, or the presence of wind crusts, among others, can significantly affect snowmelt dynamics. This might also explain why, for the 2022~~Given the above considerations and in light of our analysis, future work on the LISFLOOD snow module should focus on improving the snowfall/~~2023 season — excluded from the EO-based calibration — improvements are still present but are marginal compared to other seasons.~~ rainfall partitioning, accumulation phase, variation of snowmelt coefficient and glacier dynamics.

~~The evaluation in terms of hydrological variables leads us to conclude that no significant changes are observed. The new~~ Our findings highlight notable differences in both the spatial distribution and the magnitude of C_m across the two calibration approaches. Despite these substantial variations, the EO-based ~~snowmelt coefficient impacts~~ coefficient primarily influences the timing of snow accumulation and ~~melting phases, which, in~~ melt phases. In some cases, ~~is reflected in~~ this can affect the timing and magnitude of ~~total runoff. Although no significant differences are observed in the dischargeclimatology, the slight improvement/deterioration~~ river discharge; however, differences in KGE and ~~its components suggest that daily discharge is affected, with a surprisingly slight improvement in a few catchments. Therefore, it is reasonable to assume that recalibrating the model with EO-$C_{m,2}$ as a non-calibrated parameter could lead to an improvement of the discharge simulation. The study confirms that traditional calibration provides a satisfactory average estimation of snowmelt dynamics~~daily average discharge remain minimal in the catchments analyzed. Model results show that EFAS5 and current calibration routine generally provides a good estimation on snowmelt dynamics, on average at catchment level~~, which is beneficial for users aiming to understand the overall behavior of snow when only river dischargedata is available. Although this method performs adequately, utilizing a per-pixel calibrationoffers the~~. However, this conclusion was not obvious given the large number of calibrated parameters in LISFLOOD (14 in total) and the possibility for EFAS5 to have a parameter set that could reproduce well river discharge but not snow dynamics. A large number of parameters in distributed hydrological models can indeed results in a set of calibrated parameters that do not represent some key processes well, such as snow processes in this exercise, and instead exhibit compensation effects with other parameters in order to maximize the objective function (KGE) and the representation of a single process (river discharge).

Since calibration maximizes KGE, we do not expect lower values if the model were completely recalibrated with the EO-derived coefficient. This suggests that a two-step calibration, first constraining the snow melt coefficient with EO data followed by recalibration of the remaining parameters, could achieve similar or even improved performance in terms of KGE with the advantage of ~~aligning the model more closely with specific snow cover observations. Isolating the contribution of snowmelt to river discharge would require a more detailed, event-based analysis~~reducing equifinality. Such an approach would allow for a more realistic representation of snow processes in LISFLOOD without compromising consistency at the larger scale, which is ~~both challenging and beyond the scope of this study. Nonetheless, changes in the timing of peak accumulation and melting can have significant downstream effects, particularly in the most upstream regions of mountainous catchments with reservoirs, influencing both storagecapacity and management strategies(Förster et al., 2016)~~particularly valuable for applications in snow-dominated basins. However, given the importance of LISFLOOD at global and European level, a two-step approach would have to go through an increased number on tests.

Our NED analysis and the shift in SWE and snowmelt that occurred in the Alpine basins suggest caution when interpreting simulated discharge upstream of calibration stations. In these areas, discharge simulations using EO-derived C_m may diverge substantially from EFAS5 outputs. This divergence is particularly important for studies focused on reservoir dynamics, where inflow variability directly impacts reservoir storage, management strategies, and the timing and volume of water available for uses such as hydropower generation, irrigation, and flood control.

The method has been This study was tested over a limited time frame and period and in a small number of basins. Scaling its implementation Extending the approach to a continental scale presents several challenges, primarily would involve significant challenges, particularly due to the processing of a vast amount of data . The reference EO-SCA dataset was generated by combining large data requirements. The EO-SCF reference dataset used here combined HR and LR snow cover products, offering enhanced spatial detail while products, improving spatial detail but also increasing the complexity of managing multiple datasets. A data management. For operational large-scale implementation might require applications, alternative ready-to-use datasets , such as those explored in Appendix A. Another possible approach could involve deriving may be more practical (Appendix A). Another promising direction could be to derive the snowmelt coefficient based on current findings, leveraging pixel-wise directly from pixel-scale features such as meteorology, geography, and land cover. However, in this study, , although in our analysis no strong correlations were identified with topographical, geographical, or land cover features, as shown in Table 3 in Appendix D. The most influential feature appears to be elevation, which exhibits a negative correlation in the Adige, Arve, Salzach, and Guadalfeo river basins. This indicates that lower values of C_m are estimated for higher elevations, meaning snow persists longer at higher elevations, as expected. For the Laborec and Umeälven basins, which are relatively flat, the correlation with elevation becomes positive. The correlation with mean snow cover duration also aligns with the findings for elevation, confirming that snow lasts longer at higher elevations. However, a more in-depth investigation is needed to fully understand the underlying relationships and how the various features are inter-connected(Sec. 4.1).

Based on our findings, we suggest proposing data assimilation schemes that not only modify In conclusion, our results highlight the potential of EO data for constraining the snowmelt coefficient, which impacts melting, but also account for local errors in the accumulation phase. Several assimilation schemes have been proposed that use snow cover information to improve hydrological models (Largeron et al., 2020). However, such an exercise requires the availability of a high-quality, daily gap-filled SCA time series. In other words, integrating EO products with hydrological models to leverage the strengths of each while addressing their limitations will be critical for improving the consistency and accuracy of snow modelingbut also emphasize the need for further research given the mentioned limitations. In addition to SCF, more complementary observations such as SWE should be incorporated, and sensitivity analyses of the SCF–SWE transformation should be undertaken. In mountainous regions, discharge data from smaller upstream catchments could provide valuable benchmarks to better evaluate and refine model performance.

6 Conclusions

In this work, we assessed the performance and limitations of the LISFLOOD snow module in simulating snowmelt and snow water balances across diverse European watersheds. By leveraging a daily HR remote sensing snow cover product, our study provided valuable insights into the model's ability to reproduce accurate snow water balances and discharge predictions across varying climatic and topographical conditions. re-calibrating the snowmelt coefficient (C_m) using highly detailed EO-derived daily snow cover data from high-resolution optical sensors, we evaluated: i) how well current EFAS5 setup reproduces snow and streamflow; ii) whether EO-derived C_m improves snow process realism; and iii) the impact of such adjustments on hydrological performance across diverse European catchments.

We introduced the use of EO data, specifically derived To this purpose, we derived EO snow cover from multi-source optical sensors. The daily gap-filled SCA, obtained from MODIS and Sentinel-2 data, was used to calibrate a spatially distributed snowmelt coefficient. We implemented and evaluated an appropriate snow cover parameterization for converting SWE into SCF to effectively evaluate snow depletion. Two methods were proposed for deriving the snowmelt coefficient : a previous approach, based on the number of snow-covered days (Pistocchi et al., 2017), and a novel The snowmelt coefficient was derived through an optimization-based approach that minimizes the error between simulated and observed SCF.

The primary objective of comparing the EFAS5 setup with the same setup incorporating the independently calibrated snowmelt coefficient was to evaluate whether recalibrating this single parameter would significantly impact the hydrological cycle. Additionally, this approach enabled us to assess the robustness of the full LISFLOOD calibration—which involves 14 parameters—in accurately reproducing snow dynamics.

Our main findings indicate that the accuracy of the current current LISFLOOD snow module, which has traditionally been calibrated using a classical standard hydrological approach, already produces satisfactory results when evaluated at basin scale. When compared evaluated against EO-SCF, the model's bias ranged from -0.56% for the Guadalfeo basin to 22.50% for the Laborecbasin–0.63% (Gállego) to 22.43% (Laborec), with RMSE values varying from 20.43% for the between 20.46% (Umeälvenbasin to 54.64% for the) and 54.58% (Mörrumsånbasin). These results highlightthe misrepresentation of , however, that fractional snow cover by the current LISFLOOD setup, which can be partially corrected for the melting days by applying a is often misrepresented in the current setup. A dedicated calibration of the degree-day . We obtained improvements factor improved performance, particularly during melting periods, with gains of up to 8% both in in both bias and RMSEwhen an optimization approach is used. This method outperforms the previous approach by Pistocchi et al. (2017), which yielded even poorer results w.r.t. the standard LISFLOOD setup. Despite this improvement, modifying the snow module while keeping prior values of the calibration parameters did not lead to substantial changes in performance when comparing discharge. Despite these improvements in snow metrics, discharge simulations remained largely unchanged, reflecting the quasi-equifinal role of the snowmelt coefficient on streamflow. The main differences were observed appeared in the timing and magnitude of snow accumulation and melting, which sometimes affected the timing and magnitude of total runoff . in turn influenced the timing of runoff contributions. This shows that discharge-based calibration alone compensates for snow misrepresentations, often "getting the right result for the wrong reasons."

Shifts in snowmelt timing could have significant implications for water resources and storage. Ultimately, our findings highlight the potential of integrating models with satellite-based products to address existing limitations. By using more relevant observation data to refine specific calibration aspects, rather than relying solely on discharge, we can improve hydrological modeling and water balance predictions. While this approach reduces the need for extensive hydrological model calibration, it still requires a complex calibration process involving large EO datasets. Further research is needed to develop a regionalized approachfor In conclusion, our findings suggest that a sequential calibration approach—first adjusting the snowmelt coefficient ~~. Nonetheless, in a changing climate where earlier snowmelt patterns are becoming more prevalent, integrating directly observed SCA could improve the prediction of evolving snowpack characteristics. This approach may provide a more robust framework for understanding and adapting to shifting snowmelt dynamics. Ultimately, the relevance of the snow module performances is clearly dependent on the aim of the study and on the importance of the snow component in the water balance of the area~~using EO-derived SCA, followed by a post calibration of streamflow—can be a viable and potentially more efficient alternative. Furthermore, we find that a standard calibration on streamflow alone, followed by a post-replacement of the snowmelt coefficient based on SCA, can still yield acceptable results without the need to recalibrate the entire model.

Although our experiments focused on LISFLOOD, both the rationale and the calibration strategies are applicable to other distributed hydrological models facing similar challenges in snow-dominated catchments.

Code and data availability. The source code of LISFLOOD model is available on GitHub at https://github.com/ec-jrc/lisflood-code. LISFLOOD parameters are available at https://jeodpp.jrc.ec.europa.eu/ftp/jrc-opendata/CEMS-EFAS/LISFLOOD_static_and_parameter_maps_for_EFAS/, whereas the meteorological forcings are available at https://jeodpp.jrc.ec.europa.eu/ftp/jrc-opendata/CEMS-EFAS/meteorological_forcings/. The snow cover fraction time-series are available at https://zenodo.org/records/14961639. The code to reproduce the key results of this manuscript is available at https://github.com/vpremier/SCA4LISFLOOD.

Appendix A: Earth Observation Snow Cover Dataset

In the methodological ~~Section~~ Sec. 2.1, we saw that the approach presented by Premier et al. (2021) to creating a continuous, gap-filled daily SCA dataset relies on ~~two primary datasources, i.e., i) a LRSCF product based on optical data, and ii) HR~~multi-resolution optical data, in detail low-resolution (LR) SCF and high-resolution (HR) snow maps. A widely used operational LR ~~snow cover~~ SCF product with a long record (more than 20 years) is the MOD10A1 product derived from MODIS. Similarly, to obtain HR snow cover maps from Sentinel-2, we can utilize existing operational products such as the Copernicus Fractional Snow Cover (FSC) product. However, the use of other alternative datasets is also possible. Among others, we investigated the datasets listed in Table A1.

SnowFLAKES is also derived from Sentinel-2 and represents an alternative to FSC. It employs a more advanced algorithm, specifically the Snow extent from applying a Flexible Learning Algorithm using KErnel-based Spectral unmixing developed internally at Eurac (Barella et al., 2022). The method is based on an unsupervised machine learning algorithm. While we have observed an improvement in snow detection, particularly in challenging situations such as shadowed pixels, the algorithm is still experimental, and the maps are not yet available for operational use. Similarly, an alternative to MOD10A1 but with shorter temporal coverage (from 2012 onward) is represented by VNP10A1, while ESC-H provides an alternative with coarser spatial resolution. There are also operational products, such as GFSC and VNP10A1F, which provide gap-filled time-series to address cloud obstruction.

While many possible combinations are possible, we propose obtaining a daily gap-filled SCA by merging FSC and MOD10A1, referred ~~to here as Copernicus derived~~ here as Copernicus-derived gap-filled SCA (C-GSCA). This ensures both operational use

Table A1. Overview of snow cover products, their sources, native and resampled spatial resolutions, and temporal resolutions.

Product	Description	Reference	Spatial Resolution		Temporal
			Native	Resampled	Resolution
FSC	Fractional Snow Cover	Gascoin et al. (2019); Copernicus Land Monitoring Service (2021)	20m	2”	5d
SnowFLAKES	Snow extent from applying a Flexible Learning Algorithm	Barella et al. (2022)	20m	2”	5d
MOD10A1	MODIS/Terra Snow Cover Daily L3 Global, V61	Hall and Riggs (2021)	500m	20”	1d
VNP10A1	VIIRS/NPP Snow Cover Daily L3 Global, V2	Riggs and Hall (2023)	375m	12”	1d
ESC-H	Effective snow cover by VIS/IR radiometry	H-SAF Team (2020)	0.01°	1’	1d
GFSC	Gap-filled Fractional Snow Cover	Copernicus Land Monitoring Service (2021)	60m	2”	1d
VNP10A1F	Daily cloud-gap-filled VIIRS/NPP CGF Snow Cover L3	Riggs and Hall (2022)	375m	12”	1d

and the possibility to generate data back in time. However, for some selected basins, we tested the combination of MOD10A1 with SnowFLAKES, referred to here as ~~SnowFLAKES derived~~ SnowFLAKES-derived gap-filled SCA (S-GSCA).

Considering C-GSCA as the benchmark, we conducted an intercomparison ~~exercise~~ to assess the usability of different products, focusing on gaps primarily caused by cloud cover or satellite design. This analysis evaluates the potential of the analyzed datasets for use either as standalone inputs or within a merging approach by providing an overview of their agreement. Prior to the analysis, all products were resampled and aligned to a common grid to ensure comparability. Specifically, each product was resampled to a resolution close to that of the original data and structured as an exact submultiple of the LISFLOOD grid, as shown in Table A1.

In Fig. A1, we provide an overview of the available data for the different basins, including the average percentage of cloud-covered pixels and the total number of available images for each season. Images that are completely obstructed by clouds over the study area are excluded from these metrics. Note that, for limiting the amount of downloaded data, not all the products ~~are available~~ were tested for all the basins or seasons. This does not change the outcomes of the analysis.

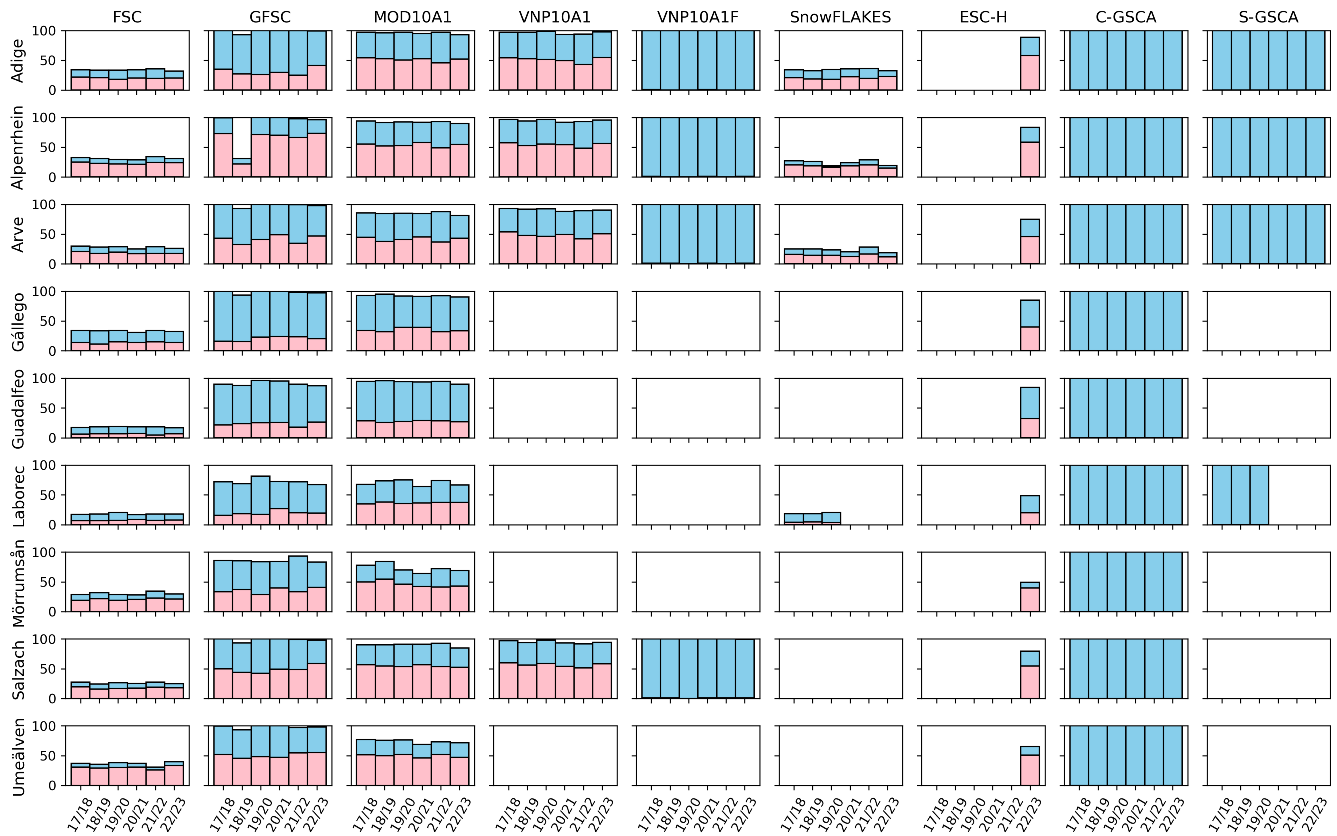

Figure A1. Overview of the available data for each basin and hydrological ~~season~~year. The percentage of available images throughout the year is shown in sky blue, while the percentage of cloud-covered pixels is represented in pink. Fully cloud-obstructed images are excluded from the calculations. Note that not all products were considered for every basin and season.

To assess the agreement or disagreement among the various datasets, we conducted an intercomparison exercise, calculating computed basic metrics such as bias, RMSE, and Pearson correlation coefficient (ρ) between pairs of datasets, using C-GSCA as the reference product. The results are reported in Fig. A2. For each matching date, metrics are calculated for SCF pixels aggregated to the final resolution of LISFLOOD. When the percentage of "no data" pixels exceeds approximately 10% within a LISFLOOD cell, SCF is marked as no data (equivalent to 90 pixels for FSC, GFSC, and SnowFLAKES; 3 pixels for VNP10A1 and VNP10A1F; and 1 pixel for MOD10A1). The figure shows the average metrics for the entire available period.

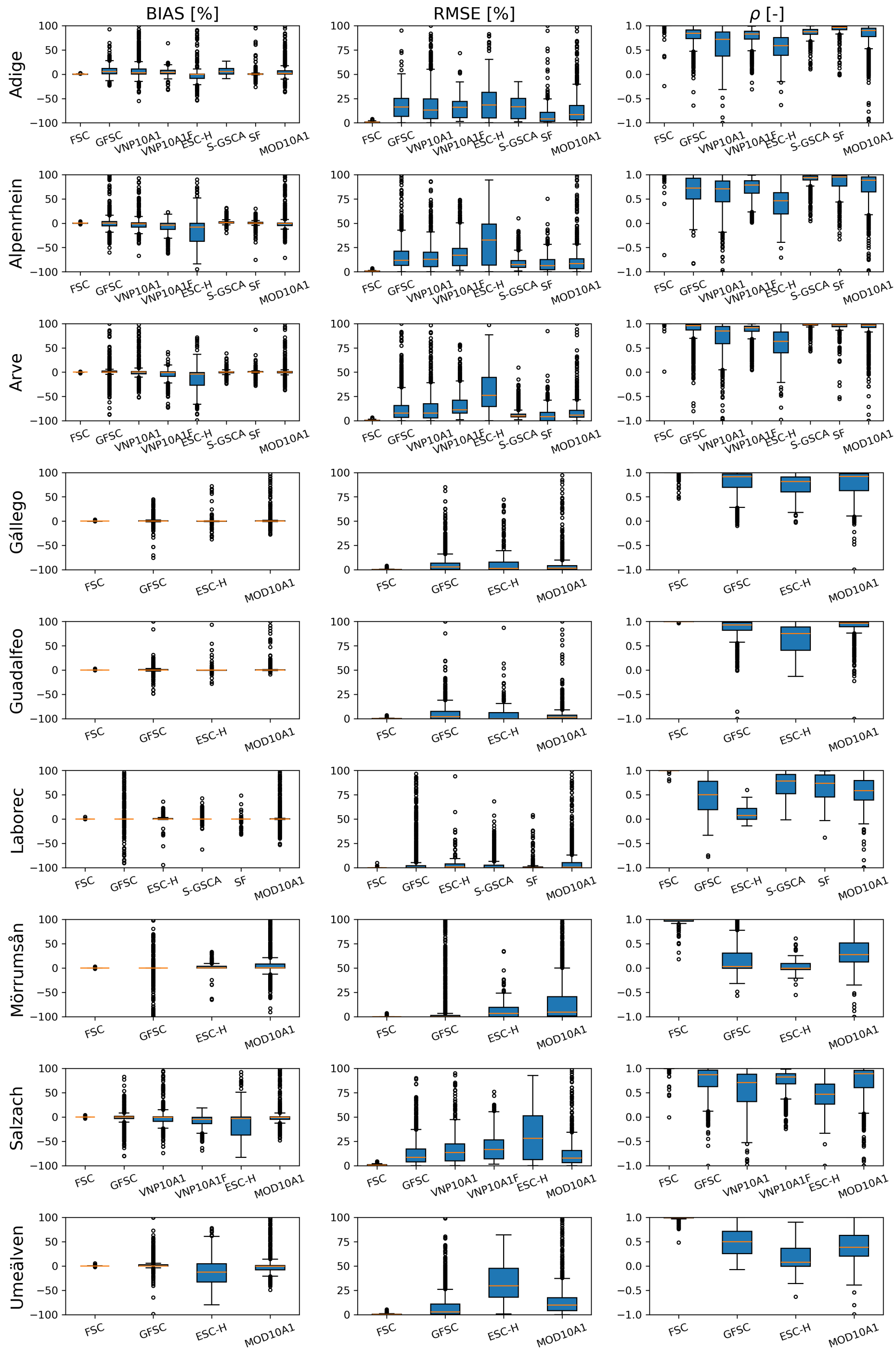

Figure A2. Boxplots of the resulting metrics (bias, RMSE and correlation) for each basin and product, using C-GSCA as the reference.

The results show that LR products (MOD10A1 and VNP10A1) offer similar image counts and metrics (on average, MOD10A1: bias 1.41%, RMSE 9.11%, and ρ 0.73, VNP10A1: bias 0.27%, RMSE 14.50%, and ρ 0.63). Note that MOD10A1 is used as input in the fusion algorithm to generate C-GSCA, but its values may be adjusted based on HR data. This results in a low bias but in the presence of outliers when compared to the benchmark (see Fig. A2). Given the similar results, VNP10A1 can be considered as a valid alternative to MOD10A1. ESC-H also exhibits comparable cloud obstruction, but shows the poorest agreement (worst metrics with bias -5.98%, RMSE 19.88%, and ρ 0.47). The results suggest that its coarser spatial resolution reduces its utility as alternative product. In general, all datasets might not be used without a proper gap-filling algorithm.

The use of HR products (such as FSC and SnowFLAKES) is significantly constrained by their low revisit frequency, which leads to limited image availability over the year. Both products show similar levels of cloud coverage and image counts. Note that SnowFLAKES has fewer images due to the application of stricter criteria in cloud masking. The lowest availability of valid pixels for FSC is observed in the Umeälven basin, with only about 6% of pixels available throughout the year. In addition to cloud obstruction, this basin is also affected by polar night, leading to missing acquisitions from November through February. However, this limitation does not impact the algorithm's performance, as the basin remains fully snow-covered during this period, and acquisitions resume in time for the snowmelt season. Alpenrhein and Salzach follow, with approximately 8% of pixels available. In contrast, the basin with the highest availability of valid pixels is Gállego with a percentage of about 19%. Since C-GSCA is derived from FSC, we expect a good agreement (bias 0.09%, RMSE 0.38% and ρ 0.99). Similar performance is also observed for SnowFLAKES (bias 0.64%, RMSE 7.11% and ρ 0.87) and S-GSCA (bias 2.53%, RMSE 9.33% and ρ 0.90), with differences due to the application of a different algorithm for the snow classification. In detail, the Adige basin exhibits a slightly higher bias. A detailed visual inspection revealed that, as also stated before, FSC tends to miss snow detection in shadowed areas. This is especially highlighted for basins with complex topography.

Regarding the gap-filled products, GFSC does not offer a valid alternative; although it provides a greater number of scenes, it still suffers from substantial "no data" gaps. The lowest availability is observed for Alpenrhein, with only around 25% of valid pixels. In fact, the gap-filling process primarily relies on propagating information from Sentinel-2 and Sentinel-1 data by using a defined temporal window (HR-S&I consortium, 2020). This is also the reason of similar performances w.r.t. the raw FSC (bias 1.18%, RMSE 10.17%, and ρ 0.72).

In contrast, the nearly complete gap-filled data in the VNP10A1F product represents an attractive option with potential applications. A tendency toward underestimation relative to the reference is shown but the metrics remain reliable (bias -3.82%, RMSE 16.66%, and ρ 0.78).

To conclude, we can state that C-GSCA is a product that by relying on HR data is expected to be more accurate w.r.t. LR data. Based on our findings, we decided to proceed with S-GSCA for the Adige basin while retaining C-GSCA for the remaining basins. In the main text, we generally refer to the time series as EO-SCA.

Appendix B: Snow Cover Parametrization

As explained In this Appendix, we provide additional details and analysis regarding the snow cover parametrization described in Sec. 2.4 , before comparing LISFLOOD results with the EO-SCA or computing the new snowmelt coefficient, an appropriate parametrization is required to convert SWE into SCF. Here we report the results obtained when considering

B1 Alternative Parametrization Approach

Here, we present results obtained using the parametrization proposed by Swenson and Lawrence (2012) (see Sec. 2.3) compared and compare them with the approach proposed introduced by Zaitchik and Rodell (2009). The following relationship is used:

$$\mathrm{SCF} = \min\left\{1 - \left[\exp\left(-\tau\frac{\mathrm{SWE}}{\mathrm{SWE}_{\mathrm{max}}}\right) - \frac{\mathrm{SWE}}{\mathrm{SWE}_{\mathrm{max}}}\exp(-\tau)\right], 1\right\} \tag{B1}$$

where τ is the snow distribution shape parameter that relates the total amount of SWE to the SCF within the pixel. We set the snow distribution shape parameter τ to 4 globally, while $\mathrm{SCF}_{\mathrm{max}}$ varies from 13 mm for bare soil to 40 mm for forests as suggested by Zaitchik and Rodell (2009).

By taking the satellite-derived EO SCF as a benchmark, we evaluated the mean bias, RMSE, and correlation for each basin by comparing the EO-SCF with the SCF generated by LISFLOOD considering the standard coefficient L-C_m under the two parametrization methods. The metrics are calculated pixel-wise and an average over time and space is computed. The results, detailed in Table B1, show improved metrics when adopting the parametrization proposed by Swenson and Lawrence (2012) for Adige, Guadalfeo and Umeälven while an improvement especially in terms of bias with the formula of Zaitchik and Rodell (2009) is shown for Alpenrhein, Arve, Laborec and Salzach while the other metrics do not show important differences. Given that the results show comparable performances and the fact that the parametrization by Swenson and Lawrence (2012) is more sophisticated, we decided to keep this approach. Therefore, all analyses and results in the main text are based on this parametrization.

B2 Calibration of the Parameter k_{accum}

Here, we present the results of the calibration of the scaling parameter k_{accum}, as described in Sec. 2.3. The outcomes are shown in Fig. B1.

Appendix C: Alternative Approach for Snowmelt Coefficient Estimation

In this study we also considered a previous simpler approach presented by Pistocchi et al. (2017) to estimate the snowmelt coefficient. Under the hypothesis of a period of continuous snow cover, we can write the following balance of snowfall and snowmelt:

$$\sum_{i=1}^{n}(P_{\mathrm{snow},i} - \mathrm{SM}_i - \mathrm{IM}_i) = 0 \tag{C1}$$

Table B1. Evaluation of LISFLOOD SCF in terms of BIAS, RMSE, and correlation using the EO-SCF as the benchmark. The standard L-C_m was utilized, with SWE converted to SCF using the parametrizations proposed by Swenson and Lawrence (2012) and Zaitchik and Rodell (2009).

	Swenson and Lawrence (2012)			Zaitchik and Rodell (2009)		
	Bias [%]	**RMSE [%]**	**ρ [-]**	**Bias [%]**	**RMSE [%]**	**ρ [-]**
Adige	9.86	35.76	0.61	19.41	41.72	0.53
Alpenrhein	−12.68	32.58	0.69	−6.52	32.13	0.67
Arve	−11.77	34.68	0.63	−5.21	34.04	0.61
Gállego	−0.63	44.31	0.52	2.74	42.03	0.57
Guadalfeo	7.22	28.08	0.33	14.23	33.17	0.33
Laborec	22.43	48.81	0.46	15.54	45.14	0.48
Mörrumsån	6.95	54.58	0.27	−8.61	49.47	0.36
Salzach	−6.96	36.89	0.67	−2.34	34.56	0.68
Umeälven	−1.21	20.46	0.59	−2.29	21.67	0.59

where n is the number of days composing the continuous snow cover period. By substituting with Eq. 2, we can derive the snowmelt coefficient

$$\text{EO-}C_m = \frac{\sum_{i=1}^{n} P_{snow,i} - \sum_{i=1}^{n} \text{IM}_i - \sum_{i=1}^{n} C_{seas}(1+0.01\cdot P_{\text{rain},i}\cdot\Delta t)(T_{avg,i}-T_m)\cdot\Delta t}{\sum_{i=1}^{n}(1+0.01\cdot P_{\text{rain},i}\cdot\Delta t)(T_{avg,i}-T_m)\cdot\Delta t} \tag{C2}$$

Note that the equation is strictly valid only for a single, uninterrupted snow period, defined as a sequence of days during which a pixel remains continuously snow-covered. It is therefore not applicable to glacierized areas, regions with perennial snow cover, or locations with multiple snow cycles such as lower altitudes. However, we follow the approach of (Pistocchi et al., 2017) and apply the equation across all snow-covered days, regardless of continuity. The periods with snow presence are detected from EO-SCF. This simplification avoids additional complexity that would arise from segmenting and analyzing multiple snow periods per pixel.

The EO-C_m values obtained with this alternative approach are shown in Fig. C1. The corresponding performance metrics, directly comparable with those in Table 4, are reported in Table C1. Overall, the results indicate poorer performance compared to the optimization-based approach adopted in this study, and in some cases also relative to the standard EFAS5 calibration. The poorer performance can be explained by the fact that this approach is tailored to conditions where pixels remain continuously snow-covered, with clearly defined accumulation and melt phases. However, as noted by Pistocchi et al. (2017), this simplifying assumption breaks down in cases of intermittent or irregular snow dynamics. Moreover, intermittent snow may also reflect uncertainties in the EO-based product, particularly during the final melt phase when patchy snow cover complicates the application of the formula. Thus, the results justify the choice of using the optimization approach.

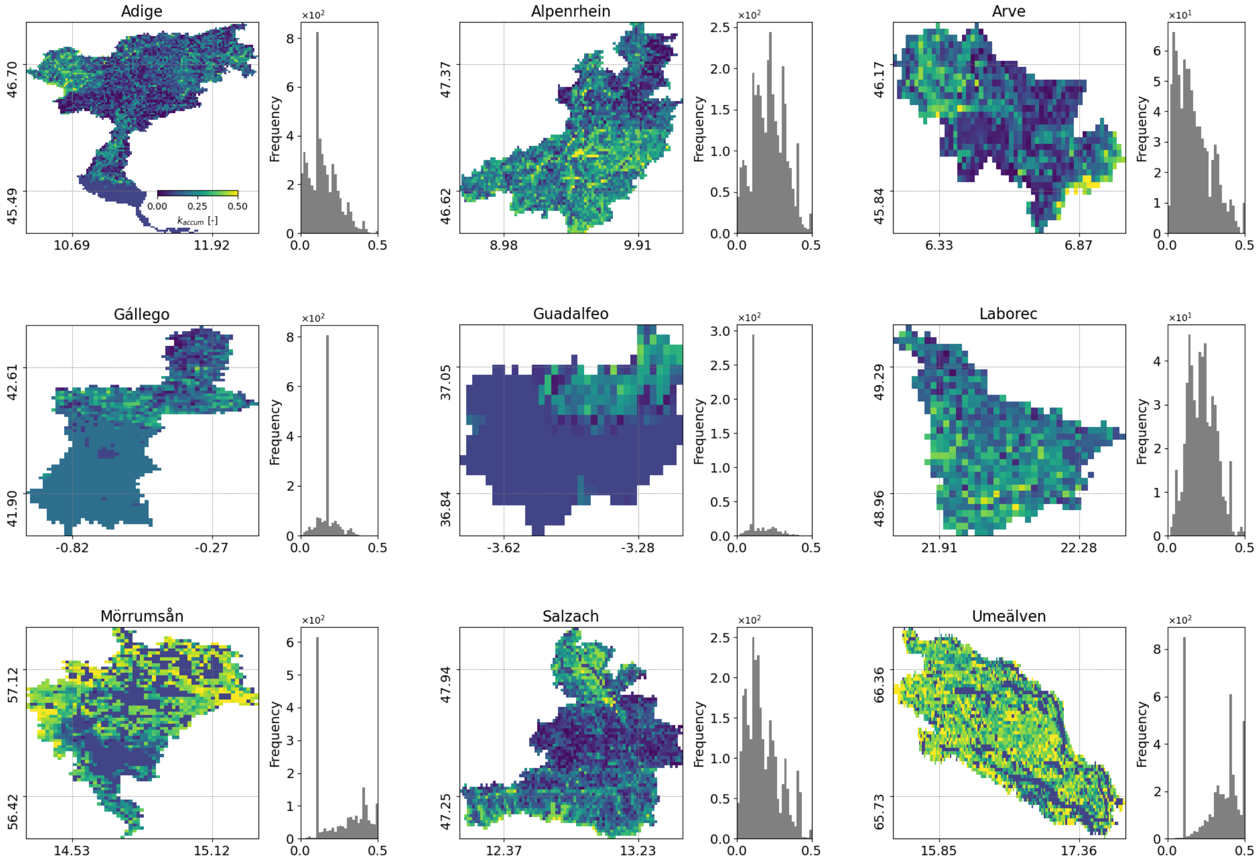

Figure B1. Scaling parameter k_{accum} for the nine selected basins. The corresponding histograms are also included.

Appendix D: Details on Snow Cover Area Evaluation

In this Appendix, we present further details that complement what was presented in Sec. 4.2.

In Table D1, the metrics obtained for each hydrological season year are reported. Again, the satellite-derived EO SCF is used as a benchmark. The metrics are calculated for three different cases: i) by using the standard LISFLOOD snowmelt coefficient by using L-C_m , ii) by considering the snowmelt coefficient obtained with the method proposed by Pistocchi et al. (2017) EO-$C_{m,1}$, and iii) by the snowmelt coefficient and EO-$C_{m,2}$ obtained by applying an optimization C_m. It should be noted that data from the 2022/23 season are completely independent since they were not utilized in the derivation of the new degree-day coefficientsoptimization but are used for validation only.

Yearly scatterplots for each basin are shown in Fig. D1 and D2.

In Table 3, the Pearson correlation coefficients between EO-$C_{m,2}$ and topographical and meteorological features, such as elevation (DEM), standard deviation of the elevation (DEM σ), slope, forest coverage, mean snow cover duration (SCD), mean

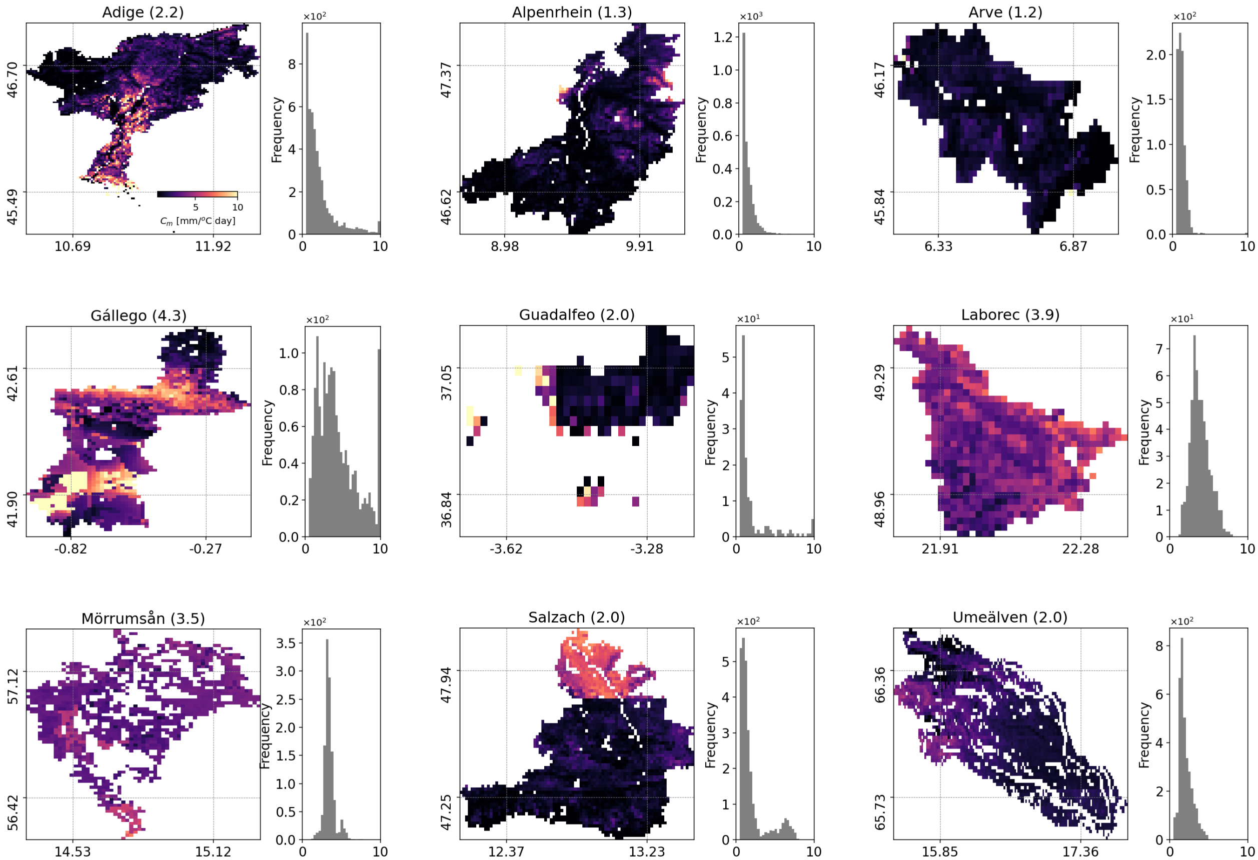

Figure C1. Snowmelt coefficients resulting from calibration against earth observation data (EO-C_m) for the nine selected basins by applying the methodology proposed by Pistocchi et al. (2017). The corresponding histograms are also included. Missing values (in white) correspond to masked areas, such as water bodies, or pixels that never experienced snow for the analysed period. Average values are reported within brackets.

~~precipitation (P) and temperature (T) - where the average is calculated for the six analysed hydrological seasons - are reported. Pearson correlation coefficients between the EO-$C_{m,2}$ and topographical, land cover and meteorological features.~~

Author contributions. FM and AP designed and conceptualized the study together with VP and CM. VP wrote the paper based on input and feedback from all coauthors. VP conducted the experiments and processing related to the SCA and the estimation of snowmelt coefficients. FM performed the experiments and processing associated with the LISFLOOD simulations. All authors contributed to the research design, as well as the discussion, analysis, and interpretation of the results.

Table C1. Evaluation of LISFLOOD SCF in terms of BIAS, RMSE, and correlation using the EO-SCF as the benchmark. The EO-based coefficient (EO-C_m) calculated with the approach of Pistocchi et al. (2017) was utilized. Pixels where both the target and reference SCF are snow-free are excluded from the analysis.

	EO-C_m		
	Bias [%]	**RMSE [%]**	**ρ [-]**
Adige	18.24	35.25	0.61
Alpenrhein	2.34	25.07	0.73
Arve	5.04	31.25	0.63
Gállego	1.42	43.66	0.54
Guadalfeo	17.24	29.55	0.36
Laborec	25.72	50.30	0.44
Mörrumsån	12.59	54.71	0.28
Salzach	7.80	30.38	0.68
Umeälven	1.66	17.68	0.65

Competing interests. The authors declare that they have no conflict of interest.

Acknowledgements. This research was supported by funding from the Joint Research Centre (JRC) through Tender No. JRC/IPR/2023/VLVP/2678 - "Support to LISFLOOD model development: testing of the snow module". We would like to acknowledge the work of our colleague Riccardo Barella (Institute for Earth Observation, Eurac Research) for providing the SnowFLAKES product, whose development was supported by the ESA Snow CCI project (Contract No. 4000124098/18/I-NB) and the ESA EXPRO+ AlpSnow - Alps Regional Initiative project (Contract No. 4000132770/20/I-NB), both financed by the European Space Agency (ESA). We also thank the CEMS Hydrological Data Collection Centre for providing the historical river discharge data.

Table D1. Evaluation of LISFLOOD SCF in terms of BIAS, RMSE, and correlation using the EO-SCF as the benchmark. The ~~standard~~ EFAS5 snowmelt coefficient (L-C_m ~~was~~) and the EO-optimized coefficient (EO-C_m) were utilized~~, with SWE converted to SCF using~~ . Pixels where both the ~~parametrizations proposed by Swenson and Lawrence (2012)~~ target and ~~Zaitchik and Rodell (2009)~~reference SCF are snow-free are excluded from the analysis.

Basin	H.y.	L-C_m Bias [%]	L-C_m RMSE [%]	L-C_m ρ [-]	EO-C_m Bias [%]	EO-C_m RMSE [%]	EO-C_m ρ [-]
Adige	17/18	11.08	34.22	0.61	9.44	31.25	0.62
	18/19	12.08	35.02	0.55	11.06	32.37	0.57
	19/20	7.88	31.59	0.59	5.23	28.78	0.60
	20/21	8.19	31.69	0.72	5.85	28.49	0.73
	21/22	6.63	33.01	0.59	6.97	30.43	0.61
	22/23	7.76	34.74	0.61	6.94	31.88	0.62
Alpenrhein	17/18	−13.56	29.84	0.72	−6.43	21.13	0.79
	18/19	−12.63	31.00	0.71	−5.81	23.38	0.77
	19/20	−13.79	32.42	0.64	−5.26	23.93	0.70
	20/21	−12.84	32.49	0.69	−4.90	24.45	0.74
	21/22	−8.33	30.35	0.70	−0.22	23.29	0.75
	22/23	−15.85	35.21	0.62	−8.42	26.91	0.69
Arve	17/18	−8.73	30.86	0.64	−3.42	27.35	0.65
	18/19	−13.53	34.05	0.63	−9.01	29.25	0.67
	19/20	−10.71	30.27	0.54	−5.01	25.29	0.58
	20/21	−13.50	34.45	0.62	−7.70	31.11	0.64
	21/22	−8.70	35.55	0.61	−1.71	29.61	0.67
	22/23	−13.29	33.73	0.68	−9.43	30.61	0.69
Gállego	17/18	26.72	43.99	0.36	23.89	41.67	0.38
	18/19	13.98	33.19	0.51	9.88	31.16	0.50
	19/20	20.82	29.18	0.47	22.32	29.17	0.42
	20/21	−6.02	47.24	0.49	−6.96	43.44	0.52
	21/22	−2.26	27.40	0.56	−6.13	26.56	0.55
	22/23	19.49	37.72	0.60	15.84	33.41	0.64
Guadalfeo	17/18	7.10	27.07	0.53	5.16	25.30	0.49
	18/19	−3.79	32.34	0.31	−4.73	31.99	0.32
	19/20	−4.85	35.15	0.38	−7.12	34.07	0.34
	20/21	4.65	31.69	0.47	2.86	30.06	0.47
	21/22	2.99	32.54	0.32	2.29	30.95	0.31
	22/23	22.27	32.68	0.27	22.59	32.59	0.25
Laborec	17/18	10.74	45.60	0.41	4.31	45.98	0.40
	18/19	12.40	36.52	0.68	1.95	34.59	0.68
	19/20	34.82	57.85	0.15	32.80	57.45	0.15
	20/21	12.74	42.51	0.57	4.47	39.67	0.60
	21/22	30.23	48.35	0.44	19.76	42.90	0.49
	22/23	44.65	61.17	0.42	38.99	58.14	0.43
Morrumsan	17/18	5.39	44.78	0.35	4.55	44.61	0.35
	18/19	35.21	53.12	0.52	34.14	52.14	0.53
	19/20	−10.09	71.06	-0.29	−11.98	70.61	-0.28
	20/21	−13.15	44.60	0.52	−14.91	46.20	0.49
	21/22	22.49	56.10	0.25	21.61	55.52	0.26
	22/23	6.23	62.79	-0.01	3.17	63.11	-0.02
Salzach	17/18	−2.02	36.33	0.69	4.46	27.59	0.74
	18/19	−8.11	30.81	0.75	−3.72	25.99	0.73
	19/20	−6.50	37.78	0.66	3.11	30.37	0.72
	20/21	−14.57	39.00	0.62	−7.61	31.80	0.67
	21/22	−2.44	34.47	0.68	4.99	26.58	0.73
	22/23	−6.53	40.42	0.63	1.48	31.83	0.70
Umealven	17/18	−0.03	19.98	0.60	0.41	19.08	0.62
	18/19	−0.94	20.11	0.66	−0.31	17.73	0.71
	19/20	−1.86	16.46	0.75	−1.57	14.57	0.78
	20/21	−1.86	16.46	0.75	−1.57	14.57	0.78
	21/22	0.15	17.00	0.56	0.63	13.35	0.64
	22/23	−3.66	25.97	0.48	−2.50	22.95	0.54

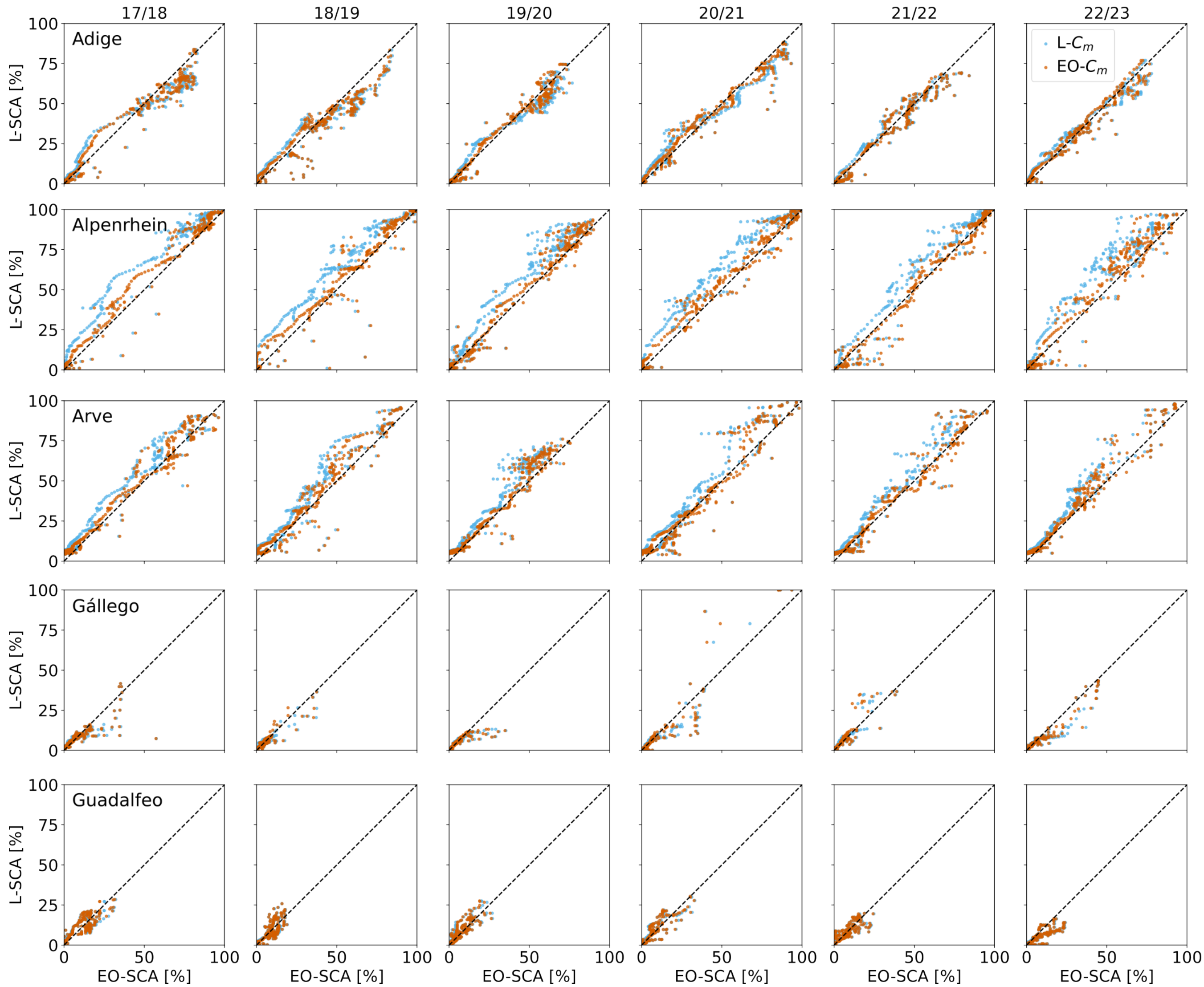

Figure D1. Scatterplots of the L-SCA obtained with the L-C_m (in cyan) ~~, EO-$C_{m,1}$ (in green)~~ and ~~$C_{m,2}$~~ EO-C_m (in orange) against EO-SCA for the Adige, Alpenrhein, Arve, Gállego, and Guadalfeo.

References

Asaoka, Y. and Kominami, Y.: Incorporation of satellite-derived snow-cover area in spatial snowmelt modeling for a large area: determination of a gridded degree-day factor, Annals of Glaciology, 54, 205–213, 2013.

Avanzi, F., Maurer, T., Glaser, S. D., Bales, R. C., and Conklin, M. H.: Information content of spatially distributed ground-based measurements for hydrologic-parameter calibration in mixed rain-snow mountain headwaters, Journal of Hydrology, 582, 124 478, 2020.

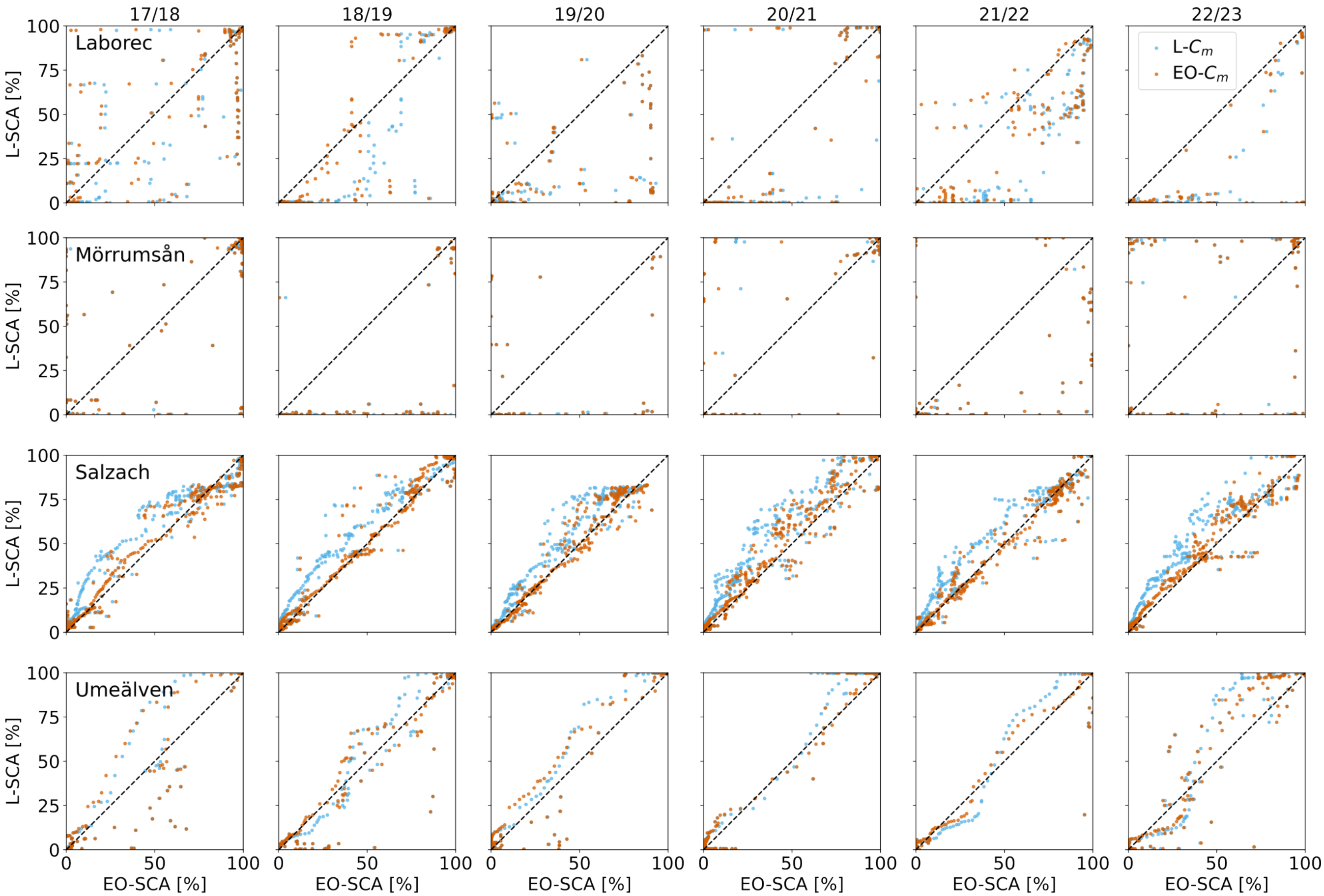

Figure D2. Scatterplots of the L-SCA obtained with the L-C_m (in cyan) ~~, EO-$C_{m,1}$ (in green)~~ and EO-~~$C_{m,2}$~~ C_m (in orange) against EO-SCA for the Laborec, Mörrumsån, Salzach and Umeälven.

Avanzi, F., Gabellani, S., Delogu, F., Silvestro, F., Pignone, F., Bruno, G., Pulvirenti, L., Squicciarino, G., Fiori, E., Rossi, L., Puca, S., Toniazzo, A., Giordano, P., Falzacappa, M., Ratto, S., Stevenin, H., Cardillo, A., Fioletti, M., Cazzuli, O., Cremonese, E., Morra di Cella, U., and Ferraris, L.: IT-SNOW: a snow reanalysis for Italy blending modeling, in-situ data, and satellite observations, https://doi.org/10.5281/zenodo.14093436, 2024.

Barella, R., Marin, C., Gianinetto, M., and Notarnicola, C.: A novel approach to high resolution snow cover fraction retrieval in mountainous regions, in: IGARSS 2022-2022 IEEE International Geoscience and Remote Sensing Symposium, pp. 3856–3859, IEEE, 2022.

Barnett, T. P., Adam, J. C., and Lettenmaier, D. P.: Potential impacts of a warming climate on water availability in snow-dominated regions, Nature, 438, 303–309, 2005.

Beck, H. E., van Dijk, A. I. J. M., de Roo, A., Miralles, D. G., McVicar, T. R., Schellekens, J., and Bruijnzeel, L. A.: Global-scale regionalization of hydrologic model parameters, Water Resour. Res., 52, 3599–3622, 2016.

Beniston, M., Stoffel, M., and Hill, M.: Impacts of climatic change on water and natural hazards in the Alps: can current water governance cope with future challenges? Examples from the European "ACQWA" project, Environmental Science & Policy, 14, 734–743, 2011.

Beven, K.: A manifesto for the equifinality thesis, J. Hydrol. (Amst.), 320, 18–36, 2006.

Beven, K.: How to make advances in hydrological modelling, Hydrol. Res., 50, 1481–1494, 2019.

Beven, K. J.: Rainfall-runoff modelling: the primer, John Wiley & Sons, 2012.

Blöschl, G., Hall, J., Parajka, J., Perdigão, R. A., Merz, B., Arheimer, B., Aronica, G. T., Bilibashi, A., Bonacci, O., Borga, M., et al.: Changing climate shifts timing of European floods, Science, 357, 588–590, 2017.

Bormann, K. J., Brown, R. D., Derksen, C., and Painter, T. H.: Estimating snow-cover trends from space, Nature Climate Change, 8, 924–928, 2018.

Burek, P., van der Knijff, J., and Roo, A. D.: LISFLOOD. Distributed Water Balance and Flood Simulation Model, https://doi.org/10.2788/24719, 2013.

Cammalleri, C., Micale, F., and Vogt, J.: On the value of combining different modelled soil moisture products for European drought monitoring, Journal of Hydrology, 525, 547–558, 2015.

Cammalleri, C., Vogt, J., and Salamon, P.: Development of an operational low-flow index for hydrological drought monitoring over Europe, Hydrological Sciences Journal, 62, 346–358, 2017.

Copernicus Land Monitoring Service: High Resolution Snow and Ice Monitoring, Online resource, https://land.copernicus.eu/pan-european/biophysical-parameters/high-resolution-snow-and-ice-monitoring, last accessed: 21 September 2024, 2021.

De Roo, A., Wesseling, C., and Deursen, W. V.: Physically based river basin modelling within a GIS: The LISFLOOD model, Hydrological Processes, 14, 1981–1992, https://doi.org/10.1002/1099-1085(20000815/30)14:11/12<1981::aid-hyp49>3.0.co;2-f, 2000.

Engel, M., Notarnicola, C., Endrizzi, S., and Bertoldi, G.: Snow model sensitivity analysis to understand spatial and temporal snow dynamics in a high-elevation catchment, Hydrological Processes, 31, 4151–4168, https://doi.org/https://doi.org/10.1002/hyp.11314, 2017.

Förster, K., Oesterle, F., Hanzer, F., Schöber, J., Huttenlau, M., and Strasser, U.: A snow and ice melt seasonal prediction modelling system for Alpine reservoirs, Proceedings of the International Association of Hydrological Sciences, 374, 143–150, https://doi.org/10.5194/piahs-374-143-2016, 2016.

Fortin, F.-A., Rainville, F.-M. D., Gardner, M.-A., Parizeau, M., and Gagné, C.: DEAP: Evolutionary Algorithms Made Easy, The Journal of Machine Learning Research, 13, 2171–2175, 2012.

Franz, K. J. and Karsten, L. R.: Calibration of a distributed snow model using MODIS snow covered area data, Journal of hydrology, 494, 160–175, 2013.

Gascoin, S., Grizonnet, M., Bouchet, M., Salgues, G., and Hagolle, O.: Theia Snow collection: High-resolution operational snow cover maps from Sentinel-2 and Landsat-8 data, Earth System Science Data, 11, 493–514, 2019.

Gyawali, D. R. and Bárdossy, A.: Development and parameter estimation of snowmelt models using spatial snow-cover observations from MODIS, Hydrology and Earth System Sciences, 26, 3055–3077, 2022.

H-SAF Team: Algorithm Theoretical Baseline Document (ATBD) for product H35 – FSC-H Effective snow cover by VIS/IR radiometry, Tech. rep., EUMETSAT H SAF, https://hsaf.meteoam.it/Products/Detail?prod=H35, 2020.

Hall, D. and Riggs, G.: MODIS/Terra Snow Cover Daily L3 Global 500m SIN Grid, Version 61, https://doi.org/10.5067/MODIS/MOD10A1.061, 2021.

Helbig, N., van Herwijnen, A., Magnusson, J., and Jonas, T.: Fractional snow-covered area parameterization over complex topography, Hydrology and Earth System Sciences, 19, 1339–1351, 2015.

HR-S&I consortium: Product User Manual for Snow Products, available at: https://land.copernicus.eu/user-corner/technical-library/hrsi-snow-pum (last access: 08 November 2024), 2020.

JRC: European Flood Awareness System v5.3, https://confluence.ecmwf.int/display/CEMS/Latest+operational+EFAS+release, 2024a.

JRC: Global Flood Awareness System v4.2, https://confluence.ecmwf.int/display/CEMS/Latest+operational+GloFAS+release, 2024b.

Kling, H., Fuchs, M., and Paulin, M.: Runoff conditions in the upper Danube basin under an ensemble of climate change scenarios, J. Hydrol. (Amst.), 424-425, 264–277, 2012.

Largeron, C., Dumont, M., Morin, S., Boone, A., Lafaysse, M., Metref, S., Cosme, E., Jonas, T., Winstral, A., and Margulis, S. A.: Toward snow cover estimation in mountainous areas using modern data assimilation methods: A review, Frontiers in Earth Science, 8, 325, 2020.

Lee, W. Y., Gim, H.-J., and Park, S. K.: Parameterizations of Snow Cover, Snow Albedo and Snow Density in Land Surface Models: A Comparative Review, Asia-Pacific Journal of Atmospheric Sciences, 60, 185–210, 2024.

Liston, G. E.: Representing subgrid snow cover heterogeneities in regional and global models, Journal of climate, 17, 1381–1397, 2004.

Martinec, J. and Rango, A.: Areal Distribution of Snow Water Equivalent Evaluated by Snow Cover Monitoring, Water Resources Research, 17, 1480–1488, https://doi.org/10.1029/WR017i005p01480, 1981.

Matthews, G., Baugh, C., Barnard, C., Carton De Wiart, C., Colonese, J., Grimaldi, S., Ham, D., Hansford, E., Harrigan, S., Heiselberg, S., Hooker, H., Hossain, S., Mazzetti, C., Milano, L., Moschini, F., O'Regan, K., Pappenberger, F., Pfister, D., Rajbhandari, R. M., Salamon, P., Ramos, A., Shelton, K., Stephens, E., Tasev, D., Turner, M., van den Homberg, M., Wittig, J., Zsótér, E., and Prudhomme, C.: Chapter 15 - On the operational implementation of the Global Flood Awareness System (GloFAS), in: Flood Forecasting (Second Edition), edited by Adams, T. E., Gangodagamage, C., and Pagano, T. C., pp. 299–350, Academic Press, second edition edn., ISBN 978-0-443-14009-9, https://doi.org/https://doi.org/10.1016/B978-0-443-14009-9.00014-6, 2025a.

Matthews, G., Baugh, C., Barnard, C., De Wiart, C. C., Colonese, J., Decremer, D., Grimaldi, S., Hansford, E., Mazzetti, C., O'Regan, K., Pappenberger, F., Ramos, A., Salamon, P., Tasev, D., and Prudhomme, C.: Chapter 14 - On the operational implementation of the European Flood Awareness System (EFAS), in: Flood Forecasting (Second Edition), edited by Adams, T. E., Gangodagamage, C., and Pagano, T. C., pp. 251–298, Academic Press, second edition edn., ISBN 978-0-443-14009-9, https://doi.org/https://doi.org/10.1016/B978-0-443-14009-9.00005-5, 2025b.

Molotch, N. P. and Margulis, S. A.: Estimating the distribution of snow water equivalent using remotely sensed snow cover data and a spatially distributed snowmelt model: A multi-resolution, multi-sensor comparison, Advances in water resources, 31, 1503–1514, 2008.

Mott, R.: Climatological snow data since 1998, OSHD, https://doi.org/http://dx.doi.org/10.16904/envidat.401, 2023.

Mott, R., Winstral, A., Cluzet, B., Helbig, N., Magnusson, J., Mazzotti, G., Quéno, L., Schirmer, M., Webster, C., and Jonas, T.: Operational snow-hydrological modeling for Switzerland, Frontiers in Earth Science, 11, 1228 158, 2023.

Niu, G.-Y. and Yang, Z.-L.: An observation-based formulation of snow cover fraction and its evaluation over large North American river basins, Journal of geophysical research: Atmospheres, 112, 2007.

Parajka, J. and Blöschl, G.: Validation of MODIS snow cover images over Austria, Hydrology and Earth System Sciences, 10, 679–689, 2006.

Pimentel, R., Herrero, J., and Polo, M. J.: Subgrid parameterization of snow distribution at a Mediterranean site using terrestrial photography, Hydrology and Earth System Sciences, 21, 805–820, 2017.

Pistocchi, A., Bagli, S., Callegari, M., Notarnicola, C., and Mazzoli, P.: On the direct calculation of snow water balances using snow cover information, Water, 9, 848, 2017.

Premier, V., Marin, C., Steger, S., Notarnicola, C., and Bruzzone, L.: A novel approach based on a hierarchical multiresolution analysis of optical time series to reconstruct the daily high-resolution snow cover area, IEEE Journal of Selected Topics in Applied Earth Observations and Remote Sensing, 14, 9223–9240, 2021.

Pulliainen, J., Luojus, K., Derksen, C., Mudryk, L., Lemmetyinen, J., Salminen, M., Ikonen, J., Takala, M., Cohen, J., Smolander, T., et al.: Patterns and trends of Northern Hemisphere snow mass from 1980 to 2018, Nature, 581, 294–298, 2020.

Riboust, P., Thirel, G., Moine, N. L., and Ribstein, P.: Revisiting a Simple Degree-Day Model for Integrating Satellite Data: Implementation of Swe-Sca Hystereses, Journal of Hydrology and Hydromechanics, 67, 70–81, https://doi.org/10.2478/johh-2018-0004, 2019.

Riggs, G. and Hall, D.: VIIRS/NPP CGF Snow Cover Daily L3 Global 375m SIN Grid, Version 2, https://doi.org/10.5067/PN50Y51IVNLE, 2022.

Riggs, G. and Hall, D.: VIIRS/NPP Snow Cover Daily L3 Global 375m SIN Grid, Version 2, https://doi.org/10.5067/45VDCKJBXWEE, 2023.

Riggs, G. A., Hall, D. K., and Román, M. O.: MODIS snow products collection 6 user guide, National Snow and Ice Data Center: Boulder, CO, USA, p. 66, 2015.

Roesch, A., Wild, M., Gilgen, H., and Ohmura, A.: A new snow cover fraction parametrization for the ECHAM4 GCM, Climate Dynamics, 17, 933–946, 2001.

Ruelland, D.: Potential of snow data to improve the consistency and robustness of a semi-distributed hydrological model using the SAFRAN input dataset, Journal of Hydrology, 631, 130 820, 2024.

Speers, D. and Versteeg, J.: Runoff forecasting for reservoir operations-the past and the future., 1982.

Swenson, S. C. and Lawrence, D.: A new fractional snow-covered area parameterization for the Community Land Model and its effect on the surface energy balance, Journal of geophysical research: Atmospheres, 117, 2012.

Takala, M., Luojus, K., Pulliainen, J., Derksen, C., Lemmetyinen, J., Kärnä, J.-P., Koskinen, J., and Bojkov, B.: Estimating northern hemisphere snow water equivalent for climate research through assimilation of space-borne radiometer data and ground-based measurements, Remote Sensing of Environment, 115, 3517–3529, 2011.

Tang, Q. and Lettenmaier, D. P.: Use of satellite snow-cover data for streamflow prediction in the Feather River Basin, California, International Journal of Remote Sensing, 31, 3745–3762, 2010.

Tedesco, M.: Remote sensing and the cryosphere, Remote Sensing of the Cryosphere, pp. 1–16, 2015.

Thiemig, V., Gomes, G. N., Skøien, J. O., Ziese, M., Rauthe-Schöch, A., Rustemeier, E., Rehfeldt, K., Walawender, J. P., Kolbe, C., Pichon, D., Schweim, C., and Salamon, P.: EMO-5: a high-resolution multi-variable gridded meteorological dataset for Europe, Earth System Science Data, 14, 3249–3272, https://doi.org/10.5194/essd-14-3249-2022, 2022.

Thirel, G., Notarnicola, C., Kalas, M., Zebisch, M., Schellenberger, T., Tetzlaff, A., Duguay, M., Mölg, N., Burek, P., and De Roo, A.: Assessing the quality of a real-time Snow Cover Area product for hydrological applications, Remote sensing of environment, 127, 271–287, 2012.

Van Der Knijff, J., Younis, J., and De Roo, A.: LISFLOOD: a GIS-based distributed model for river basin scale water balance and flood simulation, International Journal of Geographical Information Science, 24, 189–212, 2010.

Virtanen, P., Gommers, R., Oliphant, T. E., Haberland, M., Reddy, T., Cournapeau, D., Burovski, E., Peterson, P., Weckesser, W., Bright, J., van der Walt, S. J., Brett, M., Wilson, J., Millman, K. J., Mayorov, N., Nelson, A. R. J., Jones, E., Kern, R., Larson, E., Carey, C. J., Polat, İ., Feng, Y., Moore, E. W., VanderPlas, J., Laxalde, D., Perktold, J., Cimrman, R., Henriksen, I., Quintero, E. A., Harris, C. R., Archibald, A. M., Ribeiro, A. H., Pedregosa, F., van Mulbregt, P., and SciPy 1.0 Contributors: SciPy 1.0: Fundamental Algorithms for Scientific Computing in Python, Nature Methods, 17, 261–272, https://doi.org/10.1038/s41592-019-0686-2, 2020.

Viviroli, D., Dürr, H. H., Messerli, B., Meybeck, M., and Weingartner, R.: Mountains of the world, water towers for humanity: Typology, mapping, and global significance, Water resources research, 43, 2007.

Xiao, M., Mascaro, G., Wang, Z., Whitney, K. M., and Vivoni, E. R.: On the value of satellite remote sensing to reduce uncertainties of regional simulations of the Colorado River, Hydrology and Earth System Sciences, 26, 5627–5646, 2022.

Yamazaki, D., Ikeshima, D., Tawatari, R., Yamaguchi, T., O'Loughlin, F., Neal, J. C., Sampson, C. C., Kanae, S., and Bates, P. D.: A high-accuracy map of global terrain elevations, Geophysical Research Letters, 44, 5844–5853, 2017.

Zaitchik, B. F. and Rodell, M.: Forward-looking assimilation of MODIS-derived snow-covered area into a land surface model, Journal of hydrometeorology, 10, 130–148, 2009.

Zhu, Z., Tang, X., Zhang, J., Liu, L., Gao, C., Zhang, S., Wang, G., Jin, J., Liu, C., Xu, H., et al.: Enhanced runoff simulation by precise capture of snowmelt variation signals with satellite-based snow products in a high-elevation basin, Journal of Hydrology, 643, 131 920, 2024.